Physics of Fluids ARTICLE pubs.aip.org/aip/pof

Acoustic streaming outside and inside a fluid particle undergoing arbitrary axisymmetric oscillations

Cite as: Phys. Fluids 38, 043107 (2026); doi: 10.1063/5.0315990
Submitted: 10 December 2025 · Accepted: 31 March 2026 ·
Published Online: 14 April 2026

Alexander A. Doinikov,[1] Antoine Lotton,[1] Gabriel Regnault,[1] Cyril Mauger,[1] Philippe Blanc-Benon,[1] and Claude Inserra[2,a)]

AFFILIATIONS

[1]Univ Lyon, INSA Lyon, CNRS, Ecole Centrale de Lyon, Univ Claude Bernard Lyon 1, LMFA, UMR5509, 69621 Villeurbanne, France
[2]University of Lyon, Université Claude Bernard Lyon 1, Centre Léon Bérard, INSERM, UMR 1032, LabTAU, Lyon F-69003, France

[a)]Author to whom correspondence should be addressed: claude.inserra@inserm.fr

ABSTRACT

An analytical theory is developed that allows to calculate acoustic streaming outside and inside a fluid (or gas) particle immersed in another fluid (or gas) and undergoing arbitrary axisymmetric oscillations, which can include shape modes of any order. The internal and external fluids are assumed immiscible, viscous, and compressible. No restrictions are imposed on the ratio of the particle radius to the viscous penetration depth and the acoustic wavelength both outside and inside the particle. To illustrate the capabilities of the developed theory, numerical examples are provided. The results show that in the case of an air bubble in water, the gas motion inside the bubble affects the external acoustic streaming when the relative thickness of the viscous boundary layer at the bubble surface is small, a situation that occurs for large bubbles and/or high driving frequencies. In the case of a water droplet in air, more complicated steaming patterns are observed for bigger droplets. In particular, strong external near-wall vortices can develop with increasing droplet size. The results for a glycerin droplet in water also show that the streaming pattern changes noticeably with the droplet size. In particular, the direction of the main external streaming, as well as the position and the direction of rotation of near-wall vortices, can change.

I. INTRODUCTION

Interest in acoustic streaming produced by oscillating gas bubbles and liquid drops is motivated by numerous biomedical, microfluidic, and technological applications.[1–10] Acoustic streaming arises from nonlinear effect, and, as such, its mathematical description is quite a complicated problem. In order to obtain analytical solutions of this second-order mean flow, one has to solve the Navier–Stokes equations up to second-order terms in the oscillation amplitude.[11,12]

The first theoretical studies on acoustic streaming around a rigid sphere were performed by Lane,[13] Wang,[14] Riley,[15] and Gopinath.[16,17] The case of a bubble undergoing translational oscillations was first considered by Davidson and Riley,[18] and then by Wu and Du[19] and Longuet-Higgins[20] who included radial pulsations in the analysis. It is interesting to note that the acoustic streaming around a translating rigid sphere is different from that around a translating bubble even if the bubble does not undergo the radial pulsation. This difference results from the different boundary conditions at the surface of the rigid sphere (zero velocity at the interface) or at a gas bubble (zero stress at the interface). As a result, the direction of the streaming around the rigid sphere and the bubble is opposite.[14,20] Acoustic streaming produced by a bubble undergoing arbitrary axisymmetric oscillations was theoretically investigated by Maksimov,[21] Spelman and Lauga,[22] Doinikov *et al.*,[23,24] and Inserra *et al.*,[25,26] All these approaches disregard the gas motion inside the bubble and use the boundary condition of slippage at the bubble surface. Neglecting the motion of the gas inside the bubble can produce a significant change in the fluid velocities, particularly when the gas volume is large, i.e., for large bubbles, or when the thickness of the viscous boundary layer at the bubble surface is small, i.e., for high driving frequencies. While few experimental studies allowed the observation of the localized flows surrounding ultrasound contrast agents driven in MHz ultrasound fields,[27] several authors have focused on the flow surrounding bubbles with equilibrium radii of hundreds of micrometers[2,28,29] driven at relatively low frequencies (typically around 30 kHz). Only the flow outside the bubble was assessed, and disagreement was noticed on the values of the measured velocities with the existing

theoretical predictions.[30] The influence of the gas motion inside an encapsulated (contrast agent) bubble was investigated by Liu and Wu.[31] The overall streaming velocity was shown to be larger than that for a similar unencapsulated bubble for which the internal gas motion was neglected under the same ultrasound excitation, and to depend on the mechanical properties of the bubble shell and the gas. However, their analysis is limited to the case of encapsulated bubbles undergoing radial and translational oscillations. Later, Doinikov and Bouakaz[32] considered the problem of acoustic microstreaming around a gas bubble assuming the liquid outside the bubble and the gas inside to be viscous and heat-conducting. In their analysis, all modes of the bubble motion are allowed, including radial, translational, and nonspherical oscillations. However, the modal amplitudes are obtained by the approach of plane wave decomposition, meaning that these amplitudes are deduced from the applied acoustic pressure of the uniform incident wave. Such an assumption does not allow the consideration of parametric nonspherical oscillations, a situation that is usually encountered experimentally.[29,30,33]

There is an extensive literature on experimental observations of flow fields inside and outside liquid droplets. The investigation of acoustic streaming inside droplets is of considerable interest as it allows the contactless actuation of vorticity and fluid mixing through the action of an external source of ultrasound. When the droplets are located on a substrate, the excitation of sound waves inside a droplet by surface acoustic waves allows the mixing of the inner fluid,[34] the droplet displacement[35] and splitting,[36] and even the jetting[37] and atomization[38] of the inner fluid. Acoustic streaming inside a droplet can also be triggered in the case of levitated droplets trapped in a standing-wave ultrasound field. Trinh *et al.*[39] observed four counter-rotating vortices inside a droplet oscillating on mode 2 and on mode 3. Similar signatures for the streaming pattern were obtained for levitating droplets undergoing arbitrary sectorial oscillations.[40] Under microgravity conditions, the effect of the viscosity of the inner fluid on the flow arrangement was demonstrated by Yamamoto *et al.*[41] In any cases, the direct measurement of the internal fluid flows is difficult due to the small size of the droplets, the three-dimensional structure of the flow, and experimental limitations (illumination, size of the tracers and light focusing). Therefore, most studies focus on the numerical or theoretical prediction of the internal and external flows of ultrasound-driven levitated droplets.

Theoretical studies on acoustic streaming outside and inside a liquid drop undergoing translational and radial oscillations were performed by Zapryanov and Stoyanova,[42] Zhao *et al.*,[43] Rednikov *et al.*,[44] and Baasch *et al.*[45] Yarin[46] has considered acoustic streaming generated by axisymmetric shape oscillations of a droplet immersed in a host immiscible liquid. In his derivation, he considered the viscosities of both liquids to be low and uses the method of successive approximations,[47] which is based on the assumption that the thickness of the viscous boundary layers (Stokes layers) on both sides of the droplet interface is small compared to the droplet radius. Assuming a small viscous penetration depth in comparison to the bubble radius allows earlier theoretical works to introduce a matching approximation between the solution within the inner boundary layer and the one in the outer boundary. This approximation reduces the applicability of the theoretical results to the case of large bubbles in low-viscosity media. The matching approximation of the inner/outer solutions was recently removed[23] by calculating exactly the second-order mean flow induced by all possible interactions between axisymmetric shape oscillations. To the best of our knowledge, the general case of acoustic microstreaming inside and outside an oscillating droplet in an arbitrary viscous, compressible fluid, with no limitation on the ratio of the droplet radius to the viscous penetration depth and to the acoustic wavelength, both outside and inside the droplet, is still unsolved.

In the present paper, we develop an analytical theory that unites the cases of a gas bubble and a liquid drop, considering a fluid particle immersed in another fluid and undergoing arbitrary axisymmetric oscillations. This model allows one to consider radial pulsation, translation, and shape modes of any order. Our derivation is restricted to axisymmetric oscillations because a mathematical approach that would allow one to consider the case of asymmetric oscillations is currently unknown. The internal and external fluids are assumed immiscible, viscous, and compressible. With the present theory, acoustic microstreaming can be calculated both outside and inside the particle. No restrictions are imposed on the ratio of the particle radius to the viscous penetration depth and to the acoustic wavelength, both outside and inside the particle. This means that, in contrast to most earlier models, we do not assume the thickness of the outer and inner viscous boundary layer to be small compared to the particle radius and account for the compressibility of both internal and external fluids.

II. THEORY

A fluid particle, spherical at rest, immersed in another fluid, is considered. The situation applies to a gas bubble surrounded by a liquid and to a liquid drop surrounded by a gas or another liquid. The particle, which is spherical at rest, can undergo arbitrary axisymmetric oscillation modes, such as radial oscillation, translation, and shape modes of any order. Solutions to the fluid motion inside and outside the particle are expressed in the spherical coordinates (r, θ, ε), where θ is the polar angle, ε is the azimuthal angle, the origin of the coordinates is at the equilibrium center of the particle, and the z axis ($\theta = 0$) is the axis of axial symmetry (see Fig. 1).

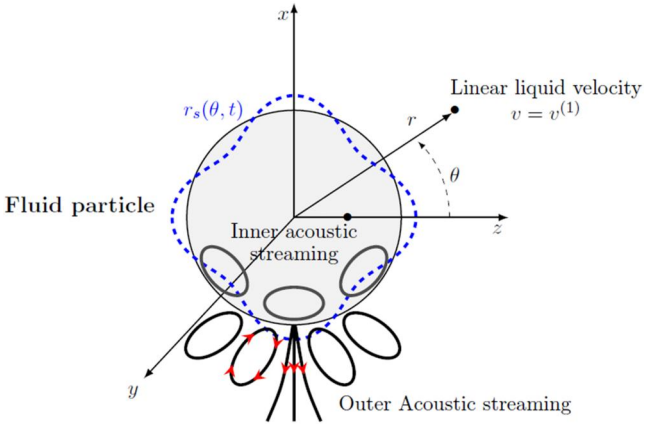

FIG. 1. Non-spherically oscillating fluid particle and illustration of the coordinate system used in calculations.

A. Basic equations

We assume the fluid motion inside and outside the particle to obey the equations of motion of a viscous compressible fluid,[48]

$$\frac{\partial \rho}{\partial t} + \nabla \cdot (\rho \boldsymbol{v}) = 0, \tag{1}$$

$$\rho\left[\frac{\partial \boldsymbol{v}}{\partial t} + (\boldsymbol{v}\cdot\nabla)\boldsymbol{v}\right] = -\nabla p + \eta\Delta\boldsymbol{v} + \left(\xi + \frac{\eta}{3}\right)\nabla(\nabla\cdot\boldsymbol{v}), \tag{2}$$

where ρ is the fluid density, $\boldsymbol{v}$ is the fluid velocity, p is the fluid pressure, η is the dynamic fluid viscosity, and ξ is the volume fluid viscosity.

Equations (1) and (2) are supplemented with the barotropic relationship,

$$p - p_0 = c^2(\rho - \rho_0), \tag{3}$$

where c is the speed of sound and p_0 and ρ_0 are, respectively, the equilibrium fluid pressure and density.

We assume that the particle undergoes N axisymmetric oscillation modes of order M_1, M_2,..., M_N. Then, the radial coordinate of the disturbed particle surface r_s can be represented by

$$r_s = R_0 + e^{-i\omega t}\sum_{m=M_1}^{M_N} s_m P_m(\mu), \tag{4}$$

where R_0 is the equilibrium radius of the particle, ω is the angular oscillation frequency, s_m is the complex amplitude of the mth mode, P_m is the Legendre polynomial of degree m, and $\mu = \cos\theta$.

The values of s_m can be taken from experimental measurements or, if parametric excitation is absent, they can be calculated analytically in terms of the amplitude of the driving acoustic pressure. They can also be computed numerically using a modeling of the bubble or drop dynamics. If a parametric excitation is investigated for instance, the system of equations ruling the modal dynamics of any shape mode can be numerically solved. Once the steady-state regime has been reached, the modal amplitudes can be replaced into the present modeling as input data.

B. First-order solutions

Keeping up to first-order terms in Eqs. (1)–(3), one obtains

$$\frac{\partial \rho_1}{\partial t} + \rho_0 \nabla\cdot\boldsymbol{v}_1 = 0, \tag{5}$$

$$\rho_0\frac{\partial \boldsymbol{v}_1}{\partial t} = -\nabla p_1 + \eta\Delta\boldsymbol{v}_1 + \left(\xi + \frac{\eta}{3}\right)\nabla(\nabla\cdot\boldsymbol{v}_1), \tag{6}$$

$$p_1 = c^2\rho_1, \tag{7}$$

where the subscript 1 means that the respective quantities are of the first order.

A solution to Eqs. (5)–(7) is sought as

$$\boldsymbol{v}_1 = \nabla\varphi_1 + \nabla\times\boldsymbol{\psi}_1, \tag{8}$$

where φ_1 and $\boldsymbol{\psi}_1$ are the first-order scalar and vector potentials, respectively.

On substitution of Eq. (8) into Eqs. (5)–(7), considering that the time dependence is $\exp(-i\omega t)$, one obtains that φ_1 and $\boldsymbol{\psi}_1$ should obey the following equations,

$$\Delta\varphi_1 + k_a^2\varphi_1 = 0, \tag{9}$$

$$\Delta\boldsymbol{\psi}_1 + k_\nu^2\boldsymbol{\psi}_1 = 0, \tag{10}$$

where the acoustic wavenumber k_a and the viscous wavenumber k_ν are given by

$$k_a = \frac{\omega}{c}\left[1 - \frac{i\omega}{\rho_0 c^2}\left(\xi + \frac{4\eta}{3}\right)\right]^{-\frac{1}{2}}, \tag{11}$$

$$k_\nu = \frac{1+i}{\delta}, \qquad \delta = \sqrt{\frac{2\nu}{\omega}}, \tag{12}$$

where $\nu = \eta/\rho_0$ is the kinematic fluid viscosity and δ is called the viscous penetration depth.

It also follows from Eqs. (5), (7), and (9) that

$$p_1 = \frac{i\rho_0 c^2 k_a^2}{\omega}\varphi_1. \tag{13}$$

In view of the axial symmetry of the problem under study, solutions to Eqs. (9) and (10) in the external fluid (outside the particle) are given by

$$\varphi_1^{(ex)}(r,\theta,t) = e^{-i\omega t}\sum_{n=0}^{\infty} a_n^{(ex)} h_n^{(1)}(k_a^{(ex)} r) P_n(\mu), \tag{14}$$

$$\boldsymbol{\psi}_1^{(ex)}(r,\theta,t) = e^{-i\omega t}\boldsymbol{e}_\varepsilon\sum_{n=1}^{\infty} b_n^{(ex)} h_n^{(1)}(k_\nu^{(ex)} r) P_n^1(\mu), \tag{15}$$

where $h_n^{(1)}$ is the spherical Hankel function of the first kind, $\boldsymbol{e}_\varepsilon$ is the unit azimuth vector, P_n^1 is the associated Legendre polynomial of the first order and degree n, $a_n^{(ex)}$ and $b_n^{(ex)}$ are the constants called linear scattering coefficients, and $k_a^{(ex)}$ and $k_\nu^{(ex)}$ are calculated by Eqs. (11) and (12) using the physical parameters of the external fluid.

On substitution of Eqs. (14) and (15) into Eq. (8), one obtains the radial and tangential components of the first-order external fluid velocity,

$$v_{1r}^{(ex)}(r,\theta,t) = \frac{e^{-i\omega t}}{r}\sum_{n=0}^{\infty}\Big[a_n^{(ex)} k_a^{(ex)} r h_n^{(1)\prime}(k_a^{(ex)} r) - b_n^{(ex)} n(n+1) h_n^{(1)}(k_\nu^{(ex)} r)\Big] P_n(\mu), \tag{16}$$

$$v_{1\theta}^{(ex)}(r,\theta,t) = \frac{e^{-i\omega t}}{r}\sum_{n=1}^{\infty}\Big\{a_n^{(ex)} h_n^{(1)}(k_a^{(ex)} r) - b_n^{(ex)}\Big[h_n^{(1)}(k_\nu^{(ex)} r) + k_\nu^{(ex)} r h_n^{(1)\prime}(k_\nu^{(ex)} r)\Big]\Big\} P_n^1(\mu), \tag{17}$$

where the prime denotes the derivative with respect to the argument in brackets.

According to Eq. (13), the first-order pressure in the external fluid is

$$p_1^{(ex)} = \frac{i\rho_0^{(ex)} c^{(ex)2} k_a^{(ex)2}}{\omega}\varphi_1^{(ex)}, \tag{18}$$

where the superscript (ex) means that the respective parameters are the parameters of the external fluid.

Solutions to Eqs. (9) and (10) in the internal fluid (inside the particle), which should be finite at $r = 0$, are given by

$$\varphi_1^{(in)}(r,\theta,t) = e^{-i\omega t}\sum_{n=0}^{\infty} a_n^{(in)} j_n(k_a^{(in)} r) P_n(\mu), \tag{19}$$

$$\boldsymbol{\psi}_1^{(in)}(r,\theta,t) = e^{-i\omega t}\boldsymbol{e}_\varepsilon \sum_{n=1}^{\infty} b_n^{(in)} j_n(k_\nu^{(in)} r) P_n^1(\mu), \tag{20}$$

where j_n is the spherical Bessel function, $a_n^{(in)}$ and $b_n^{(in)}$ are constants, and $k_a^{(in)}$ and $k_\nu^{(in)}$ are calculated by Eqs. (11) and (12) using the physical parameters of the internal fluid.

On substitution of Eqs. (19) and (20) into Eq. (8), one obtains the components of the first-order internal fluid velocity,

$$v_{1r}^{(in)}(r,\theta,t) = \frac{e^{-i\omega t}}{r}\sum_{n=0}^{\infty}\Big[a_n^{(in)} k_a^{(in)} r j_n'(k_a^{(in)} r) - b_n^{(in)} n(n+1) j_n(k_\nu^{(in)} r)\Big] P_n(\mu), \tag{21}$$

$$v_{1\theta}^{(in)}(r,\theta,t) = \frac{e^{-i\omega t}}{r}\sum_{n=1}^{\infty}\Big\{a_n^{(in)} j_n(k_a^{(in)} r) - b_n^{(in)}\Big[j_n(k_\nu^{(in)} r) + k_\nu^{(in)} r j_n'(k_\nu^{(in)} r)\Big]\Big\} P_n^1(\mu). \tag{22}$$

According to Eq. (13), the first-order pressure in the internal fluid is calculated by

$$p_1^{(in)} = \frac{i\rho_0^{(in)} c^{(in)2} k_a^{(in)2}}{\omega}\varphi_1^{(in)}, \tag{23}$$

where the superscript (in) means that the respective parameters are the parameters of the internal fluid.

Note that the equilibrium internal pressure is calculated by $p_0^{(in)} = p_0^{(ex)} + 2\sigma/R_0$, where $p_0^{(ex)}$ is the equilibrium external pressure (hydrostatic pressure) and σ is the surface tension at the particle interface. In the case of a gas bubble, the equilibrium gas density inside the bubble is calculated by $\rho_0^{(in)} = \rho_A p_0^{(in)}/p_A$, where $p_A = 101.3$ kPa is the atmospheric pressure and ρ_A is the gas density at the atmospheric pressure. In the case of a liquid drop, the equilibrium internal density $\rho_0^{(in)}$ corresponding to the pressure $p_0^{(in)}$ can be found in reference books. It should be noted that in the case of a liquid drop, the term $2\sigma/R_0$ can be neglected setting $\sigma = 0$ since a noticeable change in the liquid density requires a considerable change in the pressure, whereas the contribution of the surface tension pression, compared to the hydrostatic pressure, is negligible.

The linear scattering coefficients $a_n^{(ex)}$, $b_n^{(ex)}$, $a_n^{(in)}$, and $b_n^{(in)}$ are calculated in Appendix A by applying the boundary conditions at the particle surface given by Eqs. (A1)–(A5).

C. Equations of acoustic streaming

Keeping up to second-order terms in Eqs. (1) and (2) and averaging over time, one obtains the equations of acoustic streaming,[11]

$$\nabla\cdot\langle\rho_1\boldsymbol{v}_1\rangle + \rho_0\nabla\cdot\langle\boldsymbol{v}_2\rangle = 0, \tag{24}$$

$$\left\langle\rho_1\frac{\partial\boldsymbol{v}_1}{\partial t} + \rho_0(\boldsymbol{v}_1\cdot\nabla)\boldsymbol{v}_1\right\rangle = -\nabla\langle p_2\rangle + \eta\Delta\langle\boldsymbol{v}_2\rangle + \left(\xi+\frac{\eta}{3}\right)\nabla(\nabla\cdot\langle\boldsymbol{v}_2\rangle), \tag{25}$$

where $\langle\,\rangle$ means the time average, the subscript 2 denotes the quantities of the second order, and $\langle\boldsymbol{v}_2\rangle$ is referred to as the Eulerian velocity of acoustic streaming. Note that the time average of the time derivative of a quantity is zero, so such terms involving second-order quantities vanish in Eqs. (24) and (25).

$\langle\boldsymbol{v}_2\rangle$ is sought as

$$\langle\boldsymbol{v}_2\rangle = \nabla\Phi + \nabla\times\boldsymbol{\Psi}, \tag{26}$$

where, in view of axial symmetry, $\Phi = \Phi(r,\theta)$ and $\boldsymbol{\Psi} = \Psi(r,\theta)\boldsymbol{e}_\varepsilon$.

Substitution of Eq. (26) into Eq. (24) yields an equation for Φ,

$$\Delta\Phi = -\frac{1}{\rho_0}\nabla\cdot\langle\rho_1\boldsymbol{v}_1\rangle = -\frac{1}{2\rho_0}Re\{\nabla\cdot(\rho_1\boldsymbol{v}_1^*)\}, \tag{27}$$

where Re means "the real part of" and the asterisk denotes the complex conjugate.

With the help of Eqs. (5), (8), and (9), Eq. (27) is transformed to

$$\Delta\Phi = -\frac{1}{2\omega}Re\{\nabla\cdot(ik_a^2\varphi_1\boldsymbol{v}_1^*)\}. \tag{28}$$

Substituting Eq. (26) into Eq. (25), calculating the curl of the resulting equation, and using Eq. (5), one obtains an equation for $\boldsymbol{\Psi}$,

$$\Delta^2\boldsymbol{\Psi} = -\frac{1}{\nu}\nabla\times\langle\boldsymbol{v}_1\nabla\cdot\boldsymbol{v}_1 + \boldsymbol{v}_1\cdot\nabla\boldsymbol{v}_1\rangle. \tag{29}$$

D. Acoustic streaming produced by modes *n* and *m*

In the case where the particle oscillation can be solely decomposed over two modes, of order n and m, then Eq. (4) reduces to

$$r_s = R_0 + e^{-i\omega t}[s_n P_n(\mu) + s_m P_m(\mu)]. \tag{30}$$

Correspondingly, the first-order velocity is given by

$$\boldsymbol{v}_1 = \boldsymbol{v}_{1n} + \boldsymbol{v}_{1m}, \tag{31}$$

where

$$\boldsymbol{v}_{1n} = \nabla\varphi_{1n} + \nabla\times\boldsymbol{\psi}_{1n}, \tag{32}$$

$$\varphi_{1n} = e^{-i\omega t}a_n z_n(k_a r)P_n(\mu), \tag{33}$$

$$\boldsymbol{\psi}_{1n} = e^{-i\omega t}\boldsymbol{e}_\varepsilon b_n z_n(k_\nu r)P_n^1(\mu). \tag{34}$$

Here, z_n is $h_n^{(1)}$ for the external fluid and j_n for the internal fluid. For $\boldsymbol{v}_{1m}$, n should be replaced by m in Eqs. (32)–(34).

Equation (31) suggests that $\langle\boldsymbol{v}_2\rangle$ can be split into three parts,

$$\langle\boldsymbol{v}_2\rangle = \langle\boldsymbol{v}_2\rangle^{(nm)} + \langle\boldsymbol{v}_2\rangle^{(nn)} + \langle\boldsymbol{v}_2\rangle^{(mm)}, \tag{35}$$

where $\langle\boldsymbol{v}_2\rangle^{(nm)}$ is produced by the interaction of modes n and m, $\langle\boldsymbol{v}_2\rangle^{(nn)}$ is produced by mode n alone, and $\langle\boldsymbol{v}_2\rangle^{(mm)}$ is produced by mode m alone. Correspondingly, we have

$$\begin{aligned}\langle\boldsymbol{v}_2\rangle^{(nm)} &= \nabla\Phi^{(nm)} + \nabla\times\boldsymbol{\Psi}^{(nm)},\\ \langle\boldsymbol{v}_2\rangle^{(nn)} &= \nabla\Phi^{(nn)} + \nabla\times\boldsymbol{\Psi}^{(nn)},\\ \langle\boldsymbol{v}_2\rangle^{(mm)} &= \nabla\Phi^{(mm)} + \nabla\times\boldsymbol{\Psi}^{(mm)}.\end{aligned} \tag{36}$$

Substitution of Eq. (31) into Eqs. (28) and (29) shows that $\Phi^{(nm)}$ and $\boldsymbol{\Psi}^{(nm)}$ should obey the following equations:

$$\Delta\Phi^{(nm)} = -\frac{1}{2(1+\delta_{nm})\omega}Re\left\{\nabla\cdot\left[ik_a^2(\varphi_{1n}\boldsymbol{v}_{1m}^* + \varphi_{1m}\boldsymbol{v}_{1n}^*)\right]\right\}, \tag{37}$$

$$\Delta^2\boldsymbol{\Psi}^{(nm)} = -\frac{1}{(1+\delta_{nm})\nu}\nabla\langle\boldsymbol{v}_{1n}\nabla\cdot\boldsymbol{v}_{1m} + \boldsymbol{v}_{1m}\nabla\cdot\boldsymbol{v}_{1n} + \boldsymbol{v}_{1m}\cdot\nabla\boldsymbol{v}_{1n} + \boldsymbol{v}_{1n}\cdot\nabla\boldsymbol{v}_{1m}\rangle. \tag{38}$$

Equations (37) and (38) are valid for both $n \neq m$ and $n = m$, so they allow one to calculate all the three parts of $\langle \boldsymbol{v}_2 \rangle$. The derivation of the scalar $\Phi^{(nm)}$ and vector $\boldsymbol{\Psi}^{(nm)}$ potentials is provided in Appendix B. As a result, one obtains the components of the Eulerian streaming velocity $\boldsymbol{v}_E^{(nm)} = \langle \boldsymbol{v}_2 \rangle^{(nm)}$,

$$v_{Er}^{(nm)}(r,\theta) = \langle v_{2r} \rangle^{(nm)} = \sum_{k=1}^{n+m} \left[\Phi_k^{(nm)\prime}(r) - \frac{k(k+1)}{r} \Psi_k^{(nm)}(r) \right] P_k(\mu), \tag{39}$$

$$v_{E\theta}^{(nm)}(r,\theta) = \langle v_{2\theta} \rangle^{(nm)} = \sum_{k=1}^{n+m} \left[\frac{\Phi_k^{(nm)}(r) - \Psi_k^{(nm)}(r)}{r} - \Psi_k^{(nm)\prime}(r) \right] P_k^1(\mu), \tag{40}$$

where the functions $\Phi^{(nm)}$, $\boldsymbol{\Psi}^{(nm)}$ and their derivatives are given by Eqs. (B11), (B33), (B41), and (B42), respectively.

A complete description of acoustic streaming requires the knowledge of the Lagrangian streaming velocity, which is defined by

$$\boldsymbol{v}_L^{(nm)} = \boldsymbol{v}_E^{(nm)} + \boldsymbol{v}_S^{(nm)}, \tag{41}$$

where $\boldsymbol{v}_S^{(nm)}$ is the Stokes drift velocity.[20] The latter is calculated in Appendix C. To complete the derivation of the Lagrangian streaming velocity, it is necessary to determine all the unknown coefficients appearing in the formulation of the Eulerian velocity field. This requires to apply the appropriate boundary conditions on the Lagrangian streaming field inside the fluid particle and at its interface. This step is performed in Appendix D. To sum up, the Eulerian streaming velocity and the Stokes drift velocity are calculated by Eqs. (39), (40), (C6), and (C7). Summation of both terms gives the Lagrangian streaming velocity. The above equations are applied to both the external and the internal fluids using quantities that correspond to, respectively, the external or the internal fluid. In the most general case, where the interface deformation is decomposed over an arbitrary number of modes, all interactions are considered separately, and summed together to obtain the overall field.

E. Shear stress in the external fluid

According to Eq. (D14), the acoustic streaming generated by the interaction of modes n and m produces shear stress in the external fluid that is given by

$$\begin{aligned}\sigma_{Lr\theta}^{(nm)(ex)} = \eta^{(ex)} \sum_{k=1}^{n+m} P_k^1(\mu) \Bigg\{ & 2(k-1) r^{k-2} C_{2k}^{(nm)(ex)}(r) - \frac{2(k+2)}{r^{k+3}} \\ & \times {}^{1k(nm)(ex)}_{C}(r) - 2(k^2-1) \left[\frac{C_{3k}^{(nm)(ex)}(r)}{r^{k+1}} + r^{k-2} \right. \\ & \left. \times C_{5k}^{(nm)(ex)}(r) \right] - 2k(k+2) \left[\frac{C_{4k}^{(nm)(ex)}(r)}{r^{k+3}} + r^{k} \right. \\ & \left. \times C_{6k}^{(nm)(ex)}(r) \right] + U_{Sk}^{(nm)(ex)\prime}(r) \\ & + \frac{V_{Sk}^{(nm)(ex)}(r) - U_{Sk}^{(nm)(ex)}(r)}{r} \Bigg\},\end{aligned} \tag{42}$$

where the functions $C_{ik}^{(nm)(ex)}(r)$ are given by Eqs. (B12–B13) and (B35–B38), and the functions $U_{Sk}^{(nm)(ex)}(r)$, $V_{Sk}^{(nm)(ex)}(r)$, and $U_{Sk}^{(nm)(ex)\prime}(r)$ by Eqs. (C8), (C9), and (D23). We provide this equation because the calculation of the shear stress is of interest for a number of biomedical and technological applications.

III. NUMERICAL EXAMPLES

Numerical simulations have been performed in parallel using Mathematica and Python. The corresponding Python code is provided as supplementary material. For all the investigated cases of bubble-induced or droplet-induced streaming, qualitative comparisons with the literature will be performed when possible. Indeed, only scarce experiments are available with the simultaneous measurement of both the bubble dynamics at the acoustic timescale (allowing for the determination of the modal amplitudes of the bubble oscillations) and the microstreaming pattern. It is therefore impossible to quantitatively compare the streaming velocities predicted by our modeling with existing data, particularly inside a bubble (or inside a droplet) in which really rare observations of the internal flows exist.

A. Case of a gas bubble in water

Figures 2 and 3 illustrate the case of an air bubble in water. The following parameters were used: $\rho_0^{(ex)} = 1000\,\mathrm{kg/m^3}$, $c^{(ex)} = 1500\,\mathrm{m/s}$, $\eta^{(ex)} = 0.001\,\mathrm{Pa\ s}$, $\xi^{(ex)} = 0$, $p_0^{(ex)} = 101.3\,\mathrm{kPa}$, $\sigma = 0.0727\,\mathrm{N/m}$, $\rho_A = 1.204\,\mathrm{kg/m^3}$, $c^{(in)} = 343\,\mathrm{m/s}$, $\eta^{(in)} = 18.25\ \mu\mathrm{Pa\ s}$, and $\xi^{(in)} = 0$. The calculations were made for a bubble with radius $R_0 = 10\ \mu\mathrm{m}$ at three values of the driving frequency: $f = 30\,\mathrm{kHz}$, 300 kHz, and 1 MHz.

The results presented in Fig. 2 were obtained for modes 0 and 1, assuming $s_0 = s_1 = 1\ \mu\mathrm{m}$, i.e., oscillating in phase. This choice of the mode amplitudes, which we will also follow in other examples, is convenient because for modes of amplitudes $a\ \mu\mathrm{m}$ and $b\ \mu\mathrm{m}$, the results are simply scaled by a factor ab. Figure 2 compares the characteristics of the streaming when the gas motion inside the bubble is considered or not. Our calculations reveal that both cases are identical if the gas viscosity tends to zero, $\eta^{(in)} \to 0$. However, if the gas viscosity is nonzero, differences appear as the driving frequency increases. A similar effect is also observed if the bubble radius is increased for a fixed frequency. These findings suggest that the gas motion inside the bubble begins to affect the acoustic streaming in the liquid as the ratio δ/R_0 decreases, i.e., when the relative thickness of the viscous boundary layer at the bubble surface becomes small.

For all three frequencies considered, the streaming pattern in the liquid corresponds to the dipole flow as expected for a bubble undergoing the radial and translational oscillations.[20,23] The acoustic microstreaming inside the bubble consists of two counter-rotating vortices with velocities considerably greater than those outside the bubble.

Figure 3 shows acoustic streaming produced by the interaction of modes 0 and 2, assuming $s_0 = s_2 = 1\ \mu\mathrm{m}$. Again, the difference between the no-gas-inside case and the gas-inside case increases with increasing frequency. For all three frequencies used, the streaming pattern in the liquid corresponds to the quadrupole flow as predicted for a bubble undergoing the combination of the radial oscillation and the oblate/prolate deformation.[22,23] The streaming inside the bubble consists of four counter-rotating vortices. In contrast to the no-gas-inside case shown in Figs. 3(g)–3(i), where the spatial structure of the streaming pattern remains unchanged with increasing frequency, the streaming lobes when considering the gas inside, shown

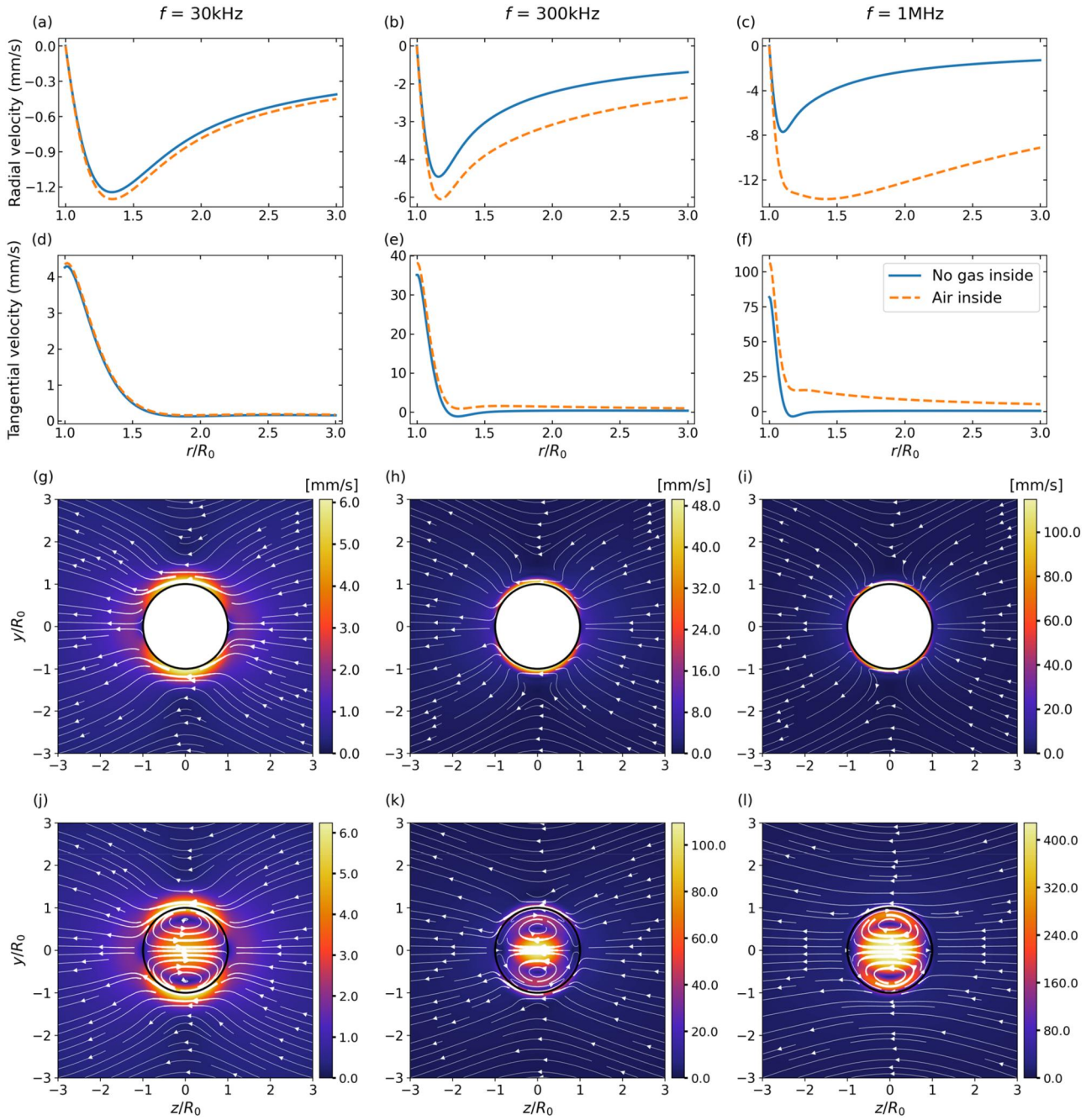

FIG. 2. Comparison of results when the gas motion inside the bubble is ignored and when the gas motion is considered. Acoustic streaming is produced by the interaction of modes 0 and 1. The gas inside the bubble is air. $R_0 = 10$ μm, $s_0 = s_1 = 1$ μm. The first, second, and third columns represent results obtained at three values of the driving frequency: $f = 30$ kHz, 300 kHz, and 1 MHz. (a)–(c) The radial component of the Lagrangian streaming velocity vs r at $\theta = \pi/4$. (d)–(f) The tangential component of the Lagrangian streaming velocity vs r at $\theta = \pi/4$. (g)–(i) Streamlines when the gas motion is ignored. (j), (k), (l) Streamlines when the gas motion is taken into account.

in Figs. 3(j)–3(l), shrink with increasing frequency, leading to an almost cross-like shape at $f = 1$ MHz.

Figure 4 compares the components of the Lagrangian streaming velocity for bubbles with different gas content: air, carbon dioxide ($\eta^{(in)} = 14.7$ μPa s, $\rho_A = 1.98$ kg/m^3, $c^{(in)} = 267$ m/s), which is present in ecological-marine and chemical processes,[49] SF6 ($\eta^{(in)} = 15$ μPa s, $\rho_A = 6.04$ kg/m^3, $c^{(in)} = 126$ m/s), which is used in microbubble ultrasound contrast agents,[50] and xenon ($\eta^{(in)} = 22.8$ μPa s, ρ_A

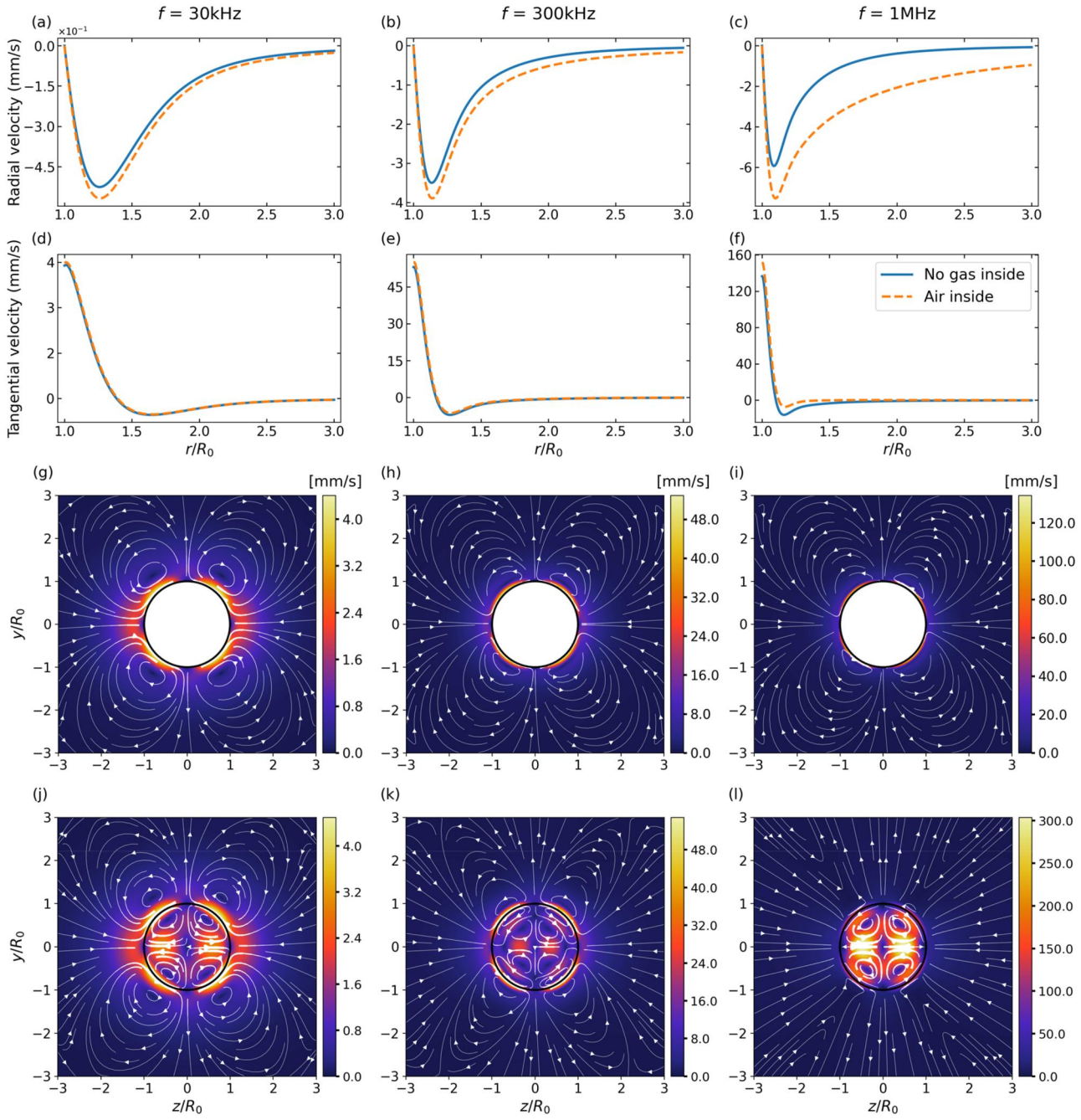

FIG. 3. Comparison of results when the gas motion inside the bubble is ignored and when the gas motion is considered. Acoustic streaming is produced by the interaction of modes 0 and 2. The gas inside the bubble is air. $R_0 = 10$ μm, $s_0 = s_2 = 1$ μm. The first, second, and third columns represent results obtained at three values of the driving frequency: $f = 30$ kHz, 300 kHz, and 1 MHz. (a)–(c) The radial component of the Lagrangian streaming velocity vs r at $\theta = \pi/4$. (d)–(f) The tangential component of the Lagrangian streaming velocity vs r at $\theta = \pi/4$. (g)–(i) Streamlines when the gas motion is ignored. (j)–(l) Streamlines when the gas motion is taken into account.

$= 5.9$ kg/m^3, $c^{(in)} = 178$ m/s), which is a noble gas used in experiments on sonoluminescence.[51] The calculations were made for a bubble with $R_0 = 10$ μm, excited at 300 kHz in water, for the cases that acoustic streaming is produced by the interaction of modes 0 and 1 with $s_0 = s_1 = 1$ μm and modes 0 and 2 with $s_0 = s_2 = 1$ μm. As one can see, the biggest difference from the no-gas-inside case is predicted for the xenon bubble, particularly when the bubble undergoes the radial and translational oscillations [Fig. 4(a)]. This means that

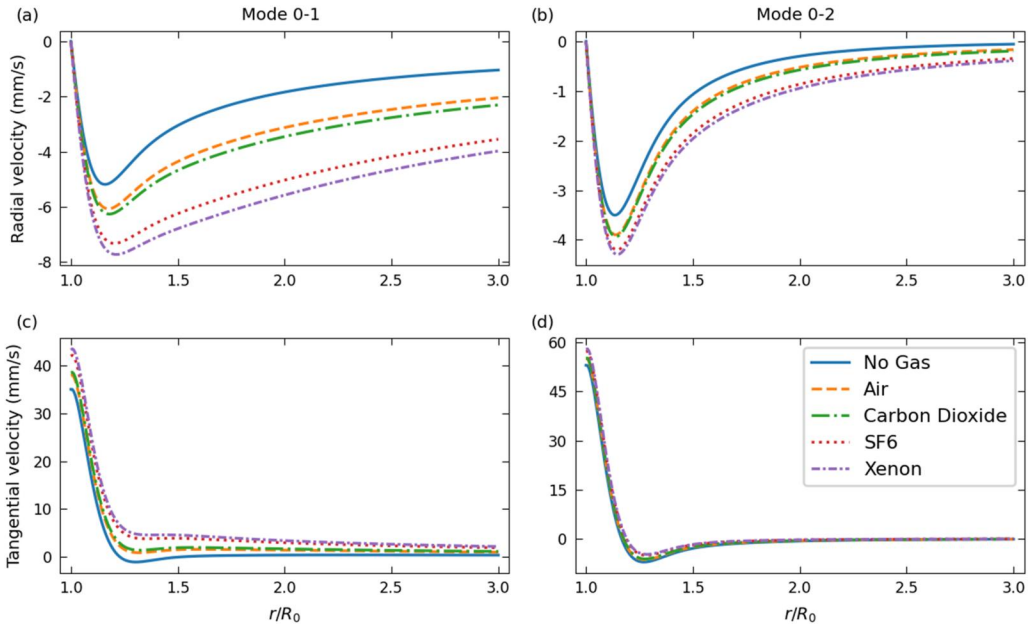

FIG. 4. The components of the Lagrangian streaming velocity for bubbles with different gas content. The external fluid is water, $R_0 = 10\ \mu$m, $f = 300$ kHz, $\theta = \pi/4$. The acoustic streaming is produced by the interaction of (a), (c) modes 0 and 1 with $s_0 = s_1 = 1\ \mu$m and (b), (d) modes 0 and 2 with $s_0 = s_2 = 1\ \mu$m.

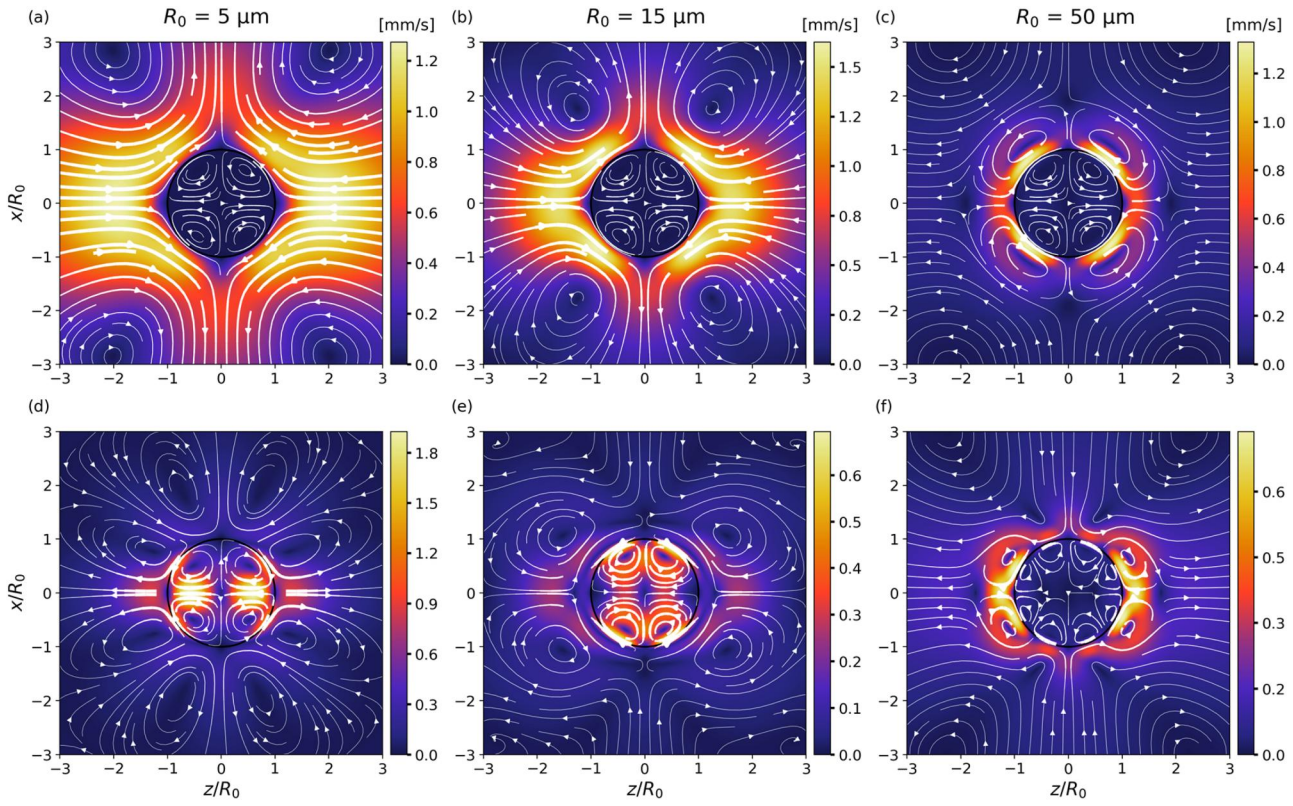

FIG. 5. Streamlines for a water droplet in air at $f = 50$ kHz for three values of R_0. (a)–(c) Streamlines produced by mode 1 with $s_1 = 1\ \mu$m. (d)–(f) Streamlines produced by mode 2 with $s_2 = 1\ \mu$m.

the intensity of the acoustic streaming depends on the gas content of the bubble and that a more vigorous streaming is generated by bubbles when the gas viscosity is considered.

B. Case of a fluid droplet surrounding by another fluid

Figure 5 illustrates the case of a water droplet in air. It shows streamlines for three values of the droplet radius (5, 15, and 50 μm) at $f = 50$ kHz. In Figs. 5(a)–5(c), streamlines produced by mode 1 are presented, i.e., streamlines produced by the interaction of mode 1 with itself. The acoustic streaming outside the droplet corresponds to the quadrupole flow, with four counter-rotating vortices whose spatial extension relatively to the droplet radius decreases when the droplet size increases. When the size of the droplet increases, strong external near-wall vortices appear [Fig. 5(c)]. Inside the bubble, the self-interaction of the translational oscillation induces four vortices, in agreement with the results of Baasch *et al.*[45] for a water droplet in oil trapped in a 1 MHz standing wave field. Agreement on the signature of the flow is obtained when the droplet is located near the velocity antinode, where the predominant contribution to the acoustic streaming results from the 1–1 interaction [Fig. 7(a) of Ref. 45].

In Figs. 5(d)–5(f), streamlines produced by mode 2 alone are presented. For small droplets, the streaming outside is constituted of eight vortices, similarly to the case of the acoustic microstreaming induced by a self-interacting mode on the interface of a gas bubble.[25] There is a strong dependence of the streaming outside the droplet on the droplet radius, because the eight-lobes pattern transforms into a cross-like pattern for a bigger droplet radius. The flow inside the droplet presents the fourfold symmetry, as observed in Shen *et al.*[40] in the case of sectorial $n = 2$ oscillations. It is worth mentioning that sectorial oscillations are asymmetric, but the sectorial $n = 2$ mode resembles an axisymmetric oblate/prolate deformation in the equatorial plane of the drop [see Fig. 4(a) of Ref. 40].

Figure 6 illustrates the case of a liquid droplet suspended in another liquid. The internal liquid is glycerin with $\eta^{(in)} = 1.48$ Pa s, $\rho_A = 1260\,\mathrm{kg/m^3}$, and $c^{(in)} = 1920$ m/s. The external liquid is water. Like Fig. 5, Fig. 6 shows streamlines produced by mode 1, Figs. 6(a)–6(c), by mode 2, Figs. 6(d)–6(f), at $f = 50$ kHz for three different equilibrium radii. As one can see, the streaming pattern changes noticeably with the droplet size. For mode 1, comparison of Figs. 6(a) and 6(c) reveals that the external streaming can change direction for different equilibrium radii: in Fig. 6(a), at $R_0 = 5$ μm, the flow is directed to the droplet surface along the z axis, whereas in Fig. 6(c), at $R_0 = 50$ μm, the flow is directed away from the droplet surface along the z axis. For mode 2, the comparison of Figs. 6(e) and 6(f) shows that both the position and the direction of rotation of the near-wall vortices are changed for different equilibrium radii: in Fig. 6(e), at

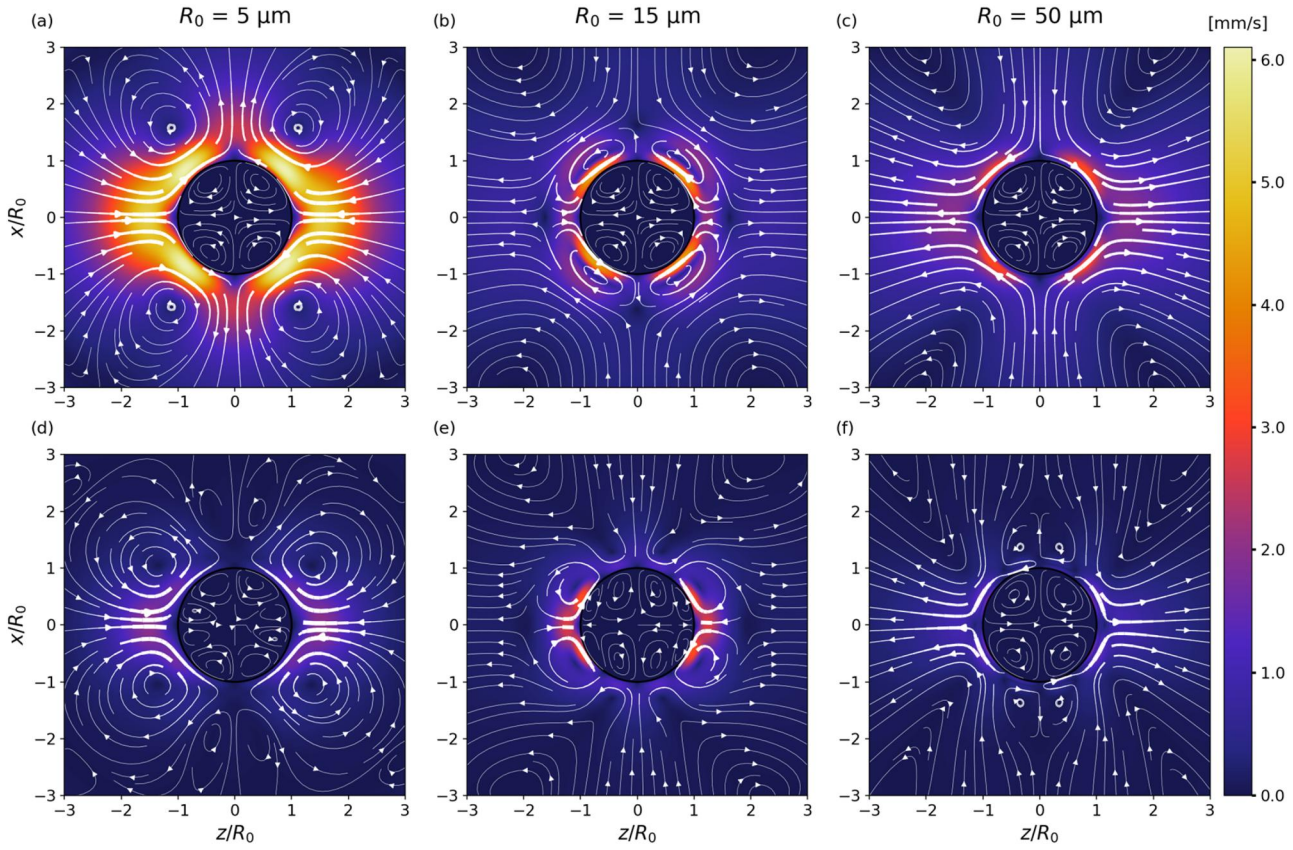

FIG. 6. Streamlines for a glycerin droplet in water at $f = 50$ kHz for three values of R_0. (a)–(c) Streamlines produced by mode 1 with $s_1 = 1$ μm. (d)–(f) Streamlines produced by mode 2 with $s_2 = 1$ μm. For comparison of the influence of the bubble radius on the streaming pattern, the velocity range is similar for all subfigures.

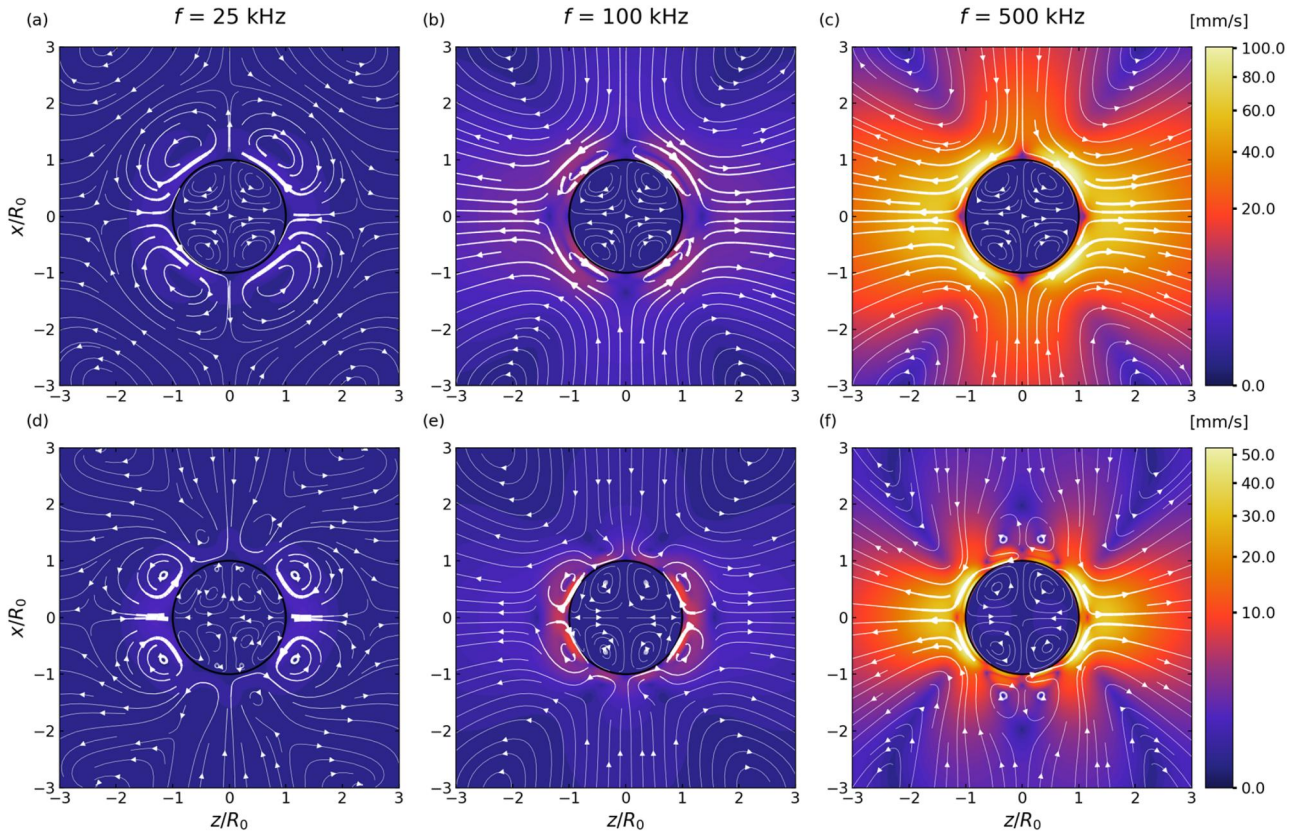

FIG. 7. Streamlines for a glycerin droplet in water at $R_0 = 15$ μm for three values of the driving frequency. (a)–(c) Streamlines produced by mode 1 with $s_1 = 1$ μm. (d)–(f) Streamlines produced by mode 2 with $s_2 = 1$ μm. For comparison of the influence of the driving frequency on the streaming pattern, the velocity range is similar for all subfigures (using a power-law dynamical range).

$R_0 = 15$ μm, the near-wall vortices are located along the z axis and rotate toward the droplet surface along this axis, whereas in Fig. 6(f), at $R_0 = 50$ μm, they are located along the x axis and rotate away from the droplet surface along this axis.

Figure 7 shows streamlines for a glycerin droplet in water for three values of the driving frequency, keeping the droplet radius constant. It gives an idea of how the streamline pattern changes with increasing frequency, i.e., with varying thickness of the viscous boundary layer. As one can see, for mode 1, the near-wall vortices become thinner as the frequency increases and the magnitude of the streaming velocity drastically increases when the driving frequency is increased. For mode 2, the near-wall vortices also become thinner. In addition, the comparison of Figs. 7(e) and 7(f) shows that additional near-wall vortices, located along the x axis, develop. When the driving frequency increases, the external streaming takes a cross-like shape with two small recirculation zones in the vicinity of the droplet interface, each of them being composed of two vortices.

IV. CONCLUSIONS

An analytical theory has been developed that allows one to calculate acoustic streaming outside and inside a fluid particle immersed in another fluid and undergoing arbitrary axisymmetric oscillations. The developed theory unites the cases of a gas bubble in a liquid and a liquid drop in a gas or another liquid. The internal and external fluids were assumed immiscible, viscous, and compressible. No restrictions were imposed on the ratio of the particle radius to the viscous penetration depth and to the acoustic wavelength both outside and inside the particle. This means that, in contrast to most previous approaches, the thickness of the outer and inner viscous boundary layer is not assumed to be small compared to the particle radius and the compressibility of both internal and external fluids is not ignored.

To illustrate the capabilities of the developed analytical theory, numerical examples were provided for the cases of a gas bubble in water, a water droplet in air, and a glycerin droplet in water. The results for a gas bubble in water show that the gas motion inside the bubble begins to affect the external acoustic streaming as the ratio δ/R_0 decreases, i.e., when the relative thickness of the viscous boundary layer at the bubble surface becomes small. The results for a water droplet in air show that more complicated steaming patterns are observed for bigger droplets. In particular, strong external near-wall vortices can develop with increasing droplet size. The results for a glycerin droplet in water also show that the streaming pattern changes noticeably with the droplet size. In particular, the direction of the

main external streaming, as well as the position and the direction of rotation of near-wall vortices, can change.

SUPPLEMENTARY MATERIAL

See the supplementary material for a Python code that allows the calculation and display of acoustic microstreaming inside and outside a fluid particle.

ACKNOWLEDGMENTS

This work was funded by l'Agence Nationale de la Recherche (ANR), project ANR-22-CE92-0062, and supported by the LabEx CeLyA of the University of Lyon (Grant No. ANR-10-LABX-0060/ANR-11-IDEX-0007).

AUTHOR DECLARATIONS

Conflict of Interest

The authors have no conflicts to disclose.

Author Contributions

Alexander A. Doinikov: Formal analysis (lead); Investigation (equal); Methodology (lead); Software (equal); Writing – original draft (lead); Writing – review & editing (lead). **Antoine Lotton:** Investigation (equal); Software (equal); Visualization (equal). **Gabriel Regnault:** Software (equal); Visualization (equal); Writing – original draft (equal). **Cyril Mauger:** Investigation (supporting); Resources (equal); Supervision (equal); Writing – review & editing (equal). **Philippe Blanc-Benon:** Investigation (supporting); Resources (equal); Supervision (equal); Writing – review & editing (equal). **Claude Inserra:** Formal analysis (equal); Investigation (equal); Methodology (equal); Project administration (lead); Software (equal); Supervision (lead); Visualization (lead); Writing – original draft (equal); Writing – review & editing (equal).

DATA AVAILABILITY

The data that support the findings of this study are available from the corresponding author upon reasonable request.

APPENDIX A: CALCULATION OF LINEAR SCATTERING COEFFICIENTS

To calculate $a_n^{(ex)}$, $b_n^{(ex)}$, $a_n^{(in)}$, and $b_n^{(in)}$, we apply the boundary conditions at the particle surface,

$$v_{1r}^{(ex)} = \frac{\partial r_s}{\partial t} \text{ at } r = R_0, \tag{A1}$$

$$v_{1r}^{(in)} = \frac{\partial r_s}{\partial t} \text{ at } r = R_0, \tag{A2}$$

$$v_{1\theta}^{(ex)} = v_{1\theta}^{(in)} \text{ at } r = R_0, \tag{A3}$$

$$\sigma_{r\theta}^{(ex)} = \sigma_{r\theta}^{(in)} \text{ at } r = R_0, \tag{A4}$$

where $\sigma_{r\theta}^{(ex,in)}$ is the tangential stress in the external and internal fluids, respectively, which is given by[48]

$$\sigma_{r\theta}^{(ex,in)} = \eta^{(ex,in)}\left(\frac{1}{r}\frac{\partial v_{1r}^{(ex,in)}}{\partial \theta} + \frac{\partial v_{1\theta}^{(ex,in)}}{\partial r} - \frac{v_{1\theta}^{(ex,in)}}{r}\right). \tag{A5}$$

Note that, since the mode amplitudes s_n are assumed to be known, there is no need in the boundary condition for the normal stress.

Substituting all the necessary quantities into the boundary conditions at the particle surface, i.e., Eqs. (A1)–(A4), one obtains for $n = 0$,

$$a_0^{(ex)} = \frac{i\omega R_0 s_0}{x_{a0}^{(ex)} h_1^{(1)}(x_{a0}^{(ex)})} \sum_{m=M_1}^{M_N} \delta_{0m}, \tag{A6}$$

$$a_0^{(in)} = \frac{i\omega R_0 s_0}{x_{a0}^{(in)} j_1(x_{a0}^{(in)})} \sum_{m=M_1}^{M_N} \delta_{0m}, \tag{A7}$$

and for $n \geq 1$

$$a_n^{(ex)} x_{a0}^{(ex)} h_n^{(1)/}(x_{a0}^{(ex)}) - b_n^{(ex)} n(n+1) h_n^{(1)}(x_{v0}^{(ex)}) = -i\omega R_0 s_n \sum_{m=M_1}^{M_N} \delta_{nm}, \tag{A8}$$

$$a_n^{(in)} x_{a0}^{(in)} j_n'(x_{a0}^{(in)}) - b_n^{(in)} n(n+1) j_n(x_{v0}^{(in)}) = -i\omega R_0 s_n \sum_{m=M_1}^{M_N} \delta_{nm}, \tag{A9}$$

$$a_n^{(ex)} h_n^{(1)}(x_{a0}^{(ex)}) - b_n^{(ex)}\left[h_n^{(1)}(x_{v0}^{(ex)}) + x_{v0}^{(ex)} h_n^{(1)/}(x_{v0}^{(ex)})\right] = a_n^{(in)} j_n(x_{a0}^{(in)}) - b_n^{(in)}\left[j_n(x_{v0}^{(in)}) + x_{v0}^{(in)} j_n'(x_{v0}^{(in)})\right], \tag{A10}$$

$$\eta^{(ex)}\left\{2a_n^{(ex)}\left[x_{a0}^{(ex)} h_n^{(1)/}(x_{a0}^{(ex)}) - h_n^{(1)}(x_{a0}^{(ex)})\right] + b_n^{(ex)}\left[(2 - n^2 - n) h_n^{(1)}(x_{v0}^{(ex)}) - x_{v0}^{(ex)2} h_n^{(1)//}(x_{v0}^{(ex)})\right]\right\} = \eta^{(in)}\left\{2a_n^{(in)}\left[x_{a0}^{(in)} j_n'(x_{a0}^{(in)}) - j_n(x_{a0}^{(in)})\right] + b_n^{(in)}\left[(2 - n^2 - n) j_n(x_{v0}^{(in)}) - x_{v0}^{(in)2} j_n''(x_{v0}^{(in)})\right]\right\}, \tag{A11}$$

where $x_{a0}^{(ex,in)} = k_a^{(ex,in)} R_0$, $x_{v0}^{(ex,in)} = k_v^{(ex,in)} R_0$, and δ_{nm} is the Kronecker delta.

From Eqs. (A8)–(A11), one finds the scattering coefficients outside and inside the particle with $n \geq 1$,

$$a_n^{(ex)} = \left[\alpha_n^{(ex)} - \beta_n^{(ex)} \frac{\eta^{(in)}}{\eta^{(ex)}} \frac{\alpha_n^{(in)}}{\beta_n^{(in)}}\right]^{-1} \left\{\frac{x_{v0}^{(ex)2} h_n^{(1)//}(x_{v0}^{(ex)})}{h_n^{(1)}(x_{v0}^{(ex)})} + (n^2 + n - 2) \times \left(1 - \frac{\eta^{(in)}}{\eta^{(ex)}}\right) + \frac{\eta^{(in)}}{\eta^{(ex)}} \frac{\alpha_n^{(in)}}{\beta_n^{(in)}}\left[\frac{x_{v0}^{(in)} j_n'(x_{v0}^{(in)})}{j_n(x_{v0}^{(in)})} - \frac{x_{v0}^{(ex)} h_n^{(1)/}(x_{v0}^{(ex)})}{h_n^{(1)}(x_{v0}^{(ex)})}\right] - \frac{\eta^{(in)}}{\eta^{(ex)}} \frac{x_{v0}^{(in)2} j_n''(x_{v0}^{(in)})}{j_n(x_{v0}^{(in)})}\right\} i\omega R_0 s_n \sum_{m=M_1}^{M_N} \delta_{nm}, \tag{A12}$$

$$b_n^{(ex)} = \frac{1}{n(n+1) h_n^{(1)}(x_{v0}^{(ex)})}\left[a_n^{(ex)} x_{a0}^{(ex)} h_n^{(1)/}(x_{a0}^{(ex)}) + i\omega R_0 s_n \sum_{m=M_1}^{M_N} \delta_{nm}\right], \tag{A13}$$

$$a_n^{(in)} = \frac{1}{\beta_n^{(in)}}\left\{a_n^{(ex)}\beta_n^{(ex)} + \left[\frac{x_{v0}^{(in)} j_n'(x_{v0}^{(in)})}{j_n(x_{v0}^{(in)})} - \frac{x_{v0}^{(ex)} h_n^{(1)\prime}(x_{v0}^{(ex)})}{h_n^{(1)}(x_{v0}^{(ex)})}\right] \times i\omega R_0 s_n \sum_{m=M_1}^{M_N}\delta_{nm}\right\}, \tag{A14}$$

$$b_n^{(in)} = \frac{1}{n(n+1)j_n(x_{v0}^{(in)})}\left[a_n^{(in)} x_{a0}^{(in)} j_n'(x_{a0}^{(in)}) + i\omega R_0 s_n \sum_{m=M_1}^{M_N}\delta_{nm}\right], \tag{A15}$$

where

$$\alpha_n^{(ex)} = (n^2+n+2)x_{a0}^{(ex)} h_n^{(1)\prime}(x_{a0}^{(ex)}) - 2n(n+1)h_n^{(1)}(x_{a0}^{(ex)}) - \frac{x_{a0}^{(ex)} x_{v0}^{(ex)2} h_n^{(1)\prime}(x_{a0}^{(ex)}) h_n^{(1)\prime\prime}(x_{v0}^{(ex)})}{h_n^{(1)}(x_{v0}^{(ex)})}, \tag{A16}$$

$$\alpha_n^{(in)} = (n^2+n+2)x_{a0}^{(in)} j_n'(x_{a0}^{(in)}) - 2n(n+1)j_n(x_{a0}^{(in)}) - \frac{x_{a0}^{(in)} x_{v0}^{(in)2} j_n'(x_{a0}^{(in)}) j_n''(x_{v0}^{(in)})}{j_n(x_{v0}^{(in)})}, \tag{A17}$$

$$\beta_n^{(ex)} = n(n+1)h_n^{(1)}(x_{a0}^{(ex)}) - x_{a0}^{(ex)} h_n^{(1)\prime}(x_{a0}^{(ex)})\left[1 + \frac{x_{v0}^{(ex)} h_n^{(1)\prime}(x_{v0}^{(ex)})}{h_n^{(1)}(x_{v0}^{(ex)})}\right], \tag{A18}$$

$$\beta_n^{(in)} = n(n+1)j_n(x_{a0}^{(in)}) - x_{a0}^{(in)} j_n'(x_{a0}^{(in)})\left[1 + \frac{x_{v0}^{(in)} j_n'(x_{v0}^{(in)})}{j_n(x_{v0}^{(in)})}\right]. \tag{A19}$$

APPENDIX B: SOLUTIONS FOR THE SCALAR AND VECTOR POTENTIALS $\Phi^{(nm)}$ AND $\Psi^{(nm)}$

The scalar $\Phi^{(nm)}$ and vector $\Psi^{(nm)}$ potentials should obey the following equations

$$\Delta\Phi^{(nm)} = -\frac{1}{2(1+\delta_{nm})\omega} Re\left\{\nabla\cdot\left[ik_a^2\left(\varphi_{1n}\boldsymbol{v}_{1m}^* + \varphi_{1m}\boldsymbol{v}_{1n}^*\right)\right]\right\}, \tag{B1}$$

$$\Delta^2\boldsymbol{\Psi}^{(nm)} = -\frac{1}{(1+\delta_{nm})\nu}\nabla\langle\boldsymbol{v}_{1n}\nabla\cdot\boldsymbol{v}_{1m} + \boldsymbol{v}_{1m}\nabla\cdot\boldsymbol{v}_{1n} + \boldsymbol{v}_{1m}\cdot\nabla\boldsymbol{v}_{1n} + \boldsymbol{v}_{1n}\cdot\nabla\boldsymbol{v}_{1m}\rangle. \tag{B2}$$

Let us first consider Eq. (B1). Calculating the divergence on the right-hand side and using Eq. (9), one obtains

$$\Delta\Phi^{(nm)} = -\frac{1}{2(1+\delta_{nm})\omega} Re\left\{ik_a^2\left(\boldsymbol{v}_{1m}^*\cdot\nabla\varphi_{1n} + \boldsymbol{v}_{1n}^*\cdot\nabla\varphi_{1m}\right)\right\}. \tag{B3}$$

Substitution of Eqs. (32)–(34) into Eq. (B3) yields

$$\Delta\Phi^{(nm)} = [A_{nm}(r) + A_{mn}(r)]P_n(\mu)P_m(\mu) + [B_{nm}(r) + B_{mn}(r)]P_n^1(\mu)P_m^1(\mu), \tag{B4}$$

where

$$A_{nm}(r) = -\frac{1}{2\omega(1+\delta_{nm})} Re\left\{ik_a^3 a_n \frac{z_n'(k_a r)}{r}\left[a_m k_a r z_m'(k_a r) - b_m m(m+1)z_m(k_\nu r)\right]^*\right\}, \tag{B5}$$

$$B_{nm}(r) = -\frac{1}{2\omega(1+\delta_{nm})} Re\left\{ik_a^2 a_n \frac{z_n(k_a r)}{r^2}\left\{a_m z_m(k_a r) - b_m\left[z_m(k_\nu r) + k_\nu r z_m'(k_\nu r)\right]\right\}^*\right\}. \tag{B6}$$

With the help of Eqs. (E6) and (E10)–(E12), Eq. (B4) is transformed to

$$\Delta\Phi^{(nm)} = \sum_{k=0}^{n+m} F_k^{(nm)}(r)P_k(\mu), \tag{B7}$$

where

$$F_k^{(nm)}(r) = [A_{nm}(r) + A_{mn}(r)]\sum_{j=|n-m|}^{n+m}\left[C_{n0m0}^{j0}\right]^2\delta_{kj} + [B_{nm}(r) + B_{mn}(r)]\frac{m(m+1)}{2m+1}(1-\delta_{n0})\sum_{j=1}^{[(n+1)/2]}(2n-4j+3) \times\left\{\sum_{s=|m-n+2j-2|}^{m+n-2j}\left[C_{(m-1)0(n-2j+1)0}^{s0}\right]^2\delta_{ks} - \sum_{s=|m-n+2j|}^{m+n-2j+2}\left[C_{(m+1)0(n-2j+1)0}^{s0}\right]^2\delta_{ks}\right\}. \tag{B8}$$

$C_{n_1m_1n_2m_2}^{n_3m_3} = \langle n_1m_1n_2m_2|n_3m_3\rangle$ are the Clebsch–Gordan coefficients,[52] and [] in the upper bound of the sum means the integer part of an expression inside the brackets.

Equation (B7) suggests that $\Phi^{(nm)}$ should be sought as

$$\Phi^{(nm)} = \sum_{k=0}^{n+m}\Phi_k^{(nm)}(r)P_k(\mu). \tag{B9}$$

Substitution of Eq. (B9) into Eq. (B7) yields

$$\Phi_k^{(nm)\prime\prime}(r) + \frac{2}{r}\Phi_k^{(nm)\prime}(r) - \frac{k(k+1)}{r^2}\Phi_k^{(nm)}(r) = F_k^{(nm)}(r). \tag{B10}$$

Equation (B10) is solved by the method of variation of constants.[35] According to this method, a solution to Eq. (B10) is written by

$$\Phi_k^{(nm)}(r) = \frac{C_{1k}^{(nm)}(r)}{r^{k+1}} + r^k C_{2k}^{(nm)}(r), \tag{B11}$$

where $C_{1k}^{(nm)}(r)$ and $C_{2k}^{(nm)}(r)$ are calculated by

$$C_{1k}^{(nm)}(r) = C_{1k0}^{(nm)} - \frac{1}{2k+1}\int_{R_0}^{r} s^{k+2}F_k^{(nm)}(s)ds, \tag{B12}$$

$$C_{2k}^{(nm)}(r) = C_{2k0}^{(nm)} + \frac{1}{2k+1}\int_{R_0}^{r} s^{1-k}F_k^{(nm)}(s)ds, \tag{B13}$$

and $C_{1k0}^{(nm)}$ and $C_{2k0}^{(nm)}$ are the constants to be determined by boundary conditions.

Let us now consider Eq. (B2). Substituting Eq. (51) into Eq. (B2) and using the identities,

$$(\boldsymbol{a}\cdot\nabla)\boldsymbol{b}+(\boldsymbol{b}\cdot\nabla)\boldsymbol{a}=\nabla(\boldsymbol{a}\cdot\boldsymbol{b})-\boldsymbol{a}\times(\nabla\times\boldsymbol{b})-\boldsymbol{b}\times(\nabla\times\boldsymbol{a}), \tag{B14}$$

$$\nabla\times(\nabla\times\boldsymbol{a})=\nabla(\nabla\cdot\boldsymbol{a})-\Delta\boldsymbol{a}, \tag{B15}$$

$$\nabla\times(c\boldsymbol{a})=c\nabla\times\boldsymbol{a}+(\nabla c)\times\boldsymbol{a}, \tag{B16}$$

$$\nabla\times(\boldsymbol{a}\times\boldsymbol{b})=(\boldsymbol{b}\cdot\nabla)\boldsymbol{a}-(\boldsymbol{a}\cdot\nabla)\boldsymbol{b}+\boldsymbol{a}(\nabla\cdot\boldsymbol{b})-\boldsymbol{b}(\nabla\cdot\boldsymbol{a}), \tag{B17}$$

and the fact that $\nabla\cdot\boldsymbol{\psi}_1=0$, one obtains

$$\begin{aligned}\Delta^2\boldsymbol{\Psi}^{(nm)}=&\frac{1}{(1+\delta_{nm})\nu}\langle 2(\Delta\varphi_{1m})\Delta\boldsymbol{\psi}_{1n}+2(\Delta\varphi_{1n})\Delta\boldsymbol{\psi}_{1m}\\&-(\nabla\Delta\varphi_{1m})\times\boldsymbol{v}_{1n}-(\nabla\Delta\varphi_{1n})\times\boldsymbol{v}_{1m}\\&-(\Delta\boldsymbol{\psi}_{1m}\cdot\nabla)\boldsymbol{v}_{1n}-(\Delta\boldsymbol{\psi}_{1n}\cdot\nabla)\boldsymbol{v}_{1m}\\&+(\boldsymbol{v}_{1n}\cdot\nabla)\Delta\boldsymbol{\psi}_{1m}+(\boldsymbol{v}_{1m}\cdot\nabla)\Delta\boldsymbol{\psi}_{1n}\rangle.\end{aligned} \tag{B18}$$

With the help of Eqs. (9) and (10), Eq. (B18) is transformed to

$$\begin{aligned}\Delta^2\boldsymbol{\Psi}^{(nm)}=&\frac{1}{2(1+\delta_{nm})\nu}Re\Big\{2k_a^2k_\nu^{2*}\left[\varphi_{1n}\boldsymbol{\psi}_{1m}^*+\varphi_{1m}\boldsymbol{\psi}_{1n}^*\right]\\&+k_a^2\left[(\nabla\varphi_{1n})\times\boldsymbol{v}_{1m}^*+(\nabla\varphi_{1m})\times\boldsymbol{v}_{1n}^*\right]\\&+k_\nu^{2*}\left[(\boldsymbol{\psi}_{1n}^*\cdot\nabla)\boldsymbol{v}_{1m}+(\boldsymbol{\psi}_{1m}^*\cdot\nabla)\boldsymbol{v}_{1n}\right.\\&\left.-(\boldsymbol{v}_{1n}\cdot\nabla)\boldsymbol{\psi}_{1m}^*-(\boldsymbol{v}_{1m}\cdot\nabla)\boldsymbol{\psi}_{1n}^*\right]\Big\}.\end{aligned} \tag{B19}$$

Substitution of Eqs. (32)–(34) into Eq. (B19) yields

$$\begin{aligned}\Delta^2\boldsymbol{\Psi}^{(nm)}=&\frac{\boldsymbol{e}_\varepsilon}{2(1+\delta_{nm})\nu}Re\Big\{D_{nm}(r)P_n(\mu)P_m^1(\mu)+D_{mn}(r)P_m(\mu)\\&\times P_n^1(\mu)+E_{nm}(r)P_n^1(\mu)\left[\cot\theta P_m^1(\mu)+\sin\theta P_m^{1\prime}(\mu)\right]\\&+E_{mn}P_m^1(\mu)\left[\cot\theta P_n^1(\mu)+\sin\theta P_n^{1\prime}(\mu)\right]\Big\},\end{aligned} \tag{B20}$$

where

$$\begin{aligned}D_{nm}(r)=&k_a^2a_n\left[2k_\nu^{2*}b_m^*z_n(k_ar)z_m^*(k_\nu r)+k_az_n'(k_ar)U_m^*(r)\right]\\&+\frac{V_n(r)}{r}\left\{k_\nu^2b_m\left[z_m(k_\nu r)-k_\nu rz_m'(k_\nu r)\right]-k_a^2a_mz_m(k_ar)\right\}^*,\end{aligned} \tag{B21}$$

$$E_{nm}(r)=\frac{U_n(r)}{r}\left[b_mk_\nu^2z_m(k_\nu r)\right]^*, \tag{B22}$$

$$V_n(r)=a_nk_az_n'(k_ar)-b_nn(n+1)\frac{z_n(k_\nu r)}{r}, \tag{B23}$$

$$U_n(r)=a_n\frac{z_n(k_ar)}{r}-b_n\left[\frac{z_n(k_\nu r)}{r}+k_\nu z_n'(k_\nu r)\right]. \tag{B24}$$

With the help of Eqs. (E7) and (E13), Eq. (B19) is transformed to

$$\Delta^2\boldsymbol{\Psi}^{(nm)}=\boldsymbol{e}_\varepsilon\sum_{k=1}^{n+m}G_k^{(nm)}(r)P_k^1(\mu), \tag{B25}$$

where

$$G_k^{(nm)}(r)=H_{knm}(r)+H_{kmn}(r)+I_{knm}(r)+I_{kmn}(r), \tag{B26}$$

$$\begin{aligned}H_{knm}(r)=&\frac{\sqrt{m(m+1)}}{2\nu(1+\delta_{nm})}Re\left\{D_{nm}(r)+n(n-1)E_{mn}(r)\right\}\\&\times\sum_{j=j_{\min}}^{n+m}\frac{C_{n0m0}^{j0}C_{n0m1}^{j1}}{\sqrt{j(j+1)}}\delta_{kj},\end{aligned} \tag{B27}$$

$$\begin{aligned}I_{knm}(r)=&-\frac{\sqrt{m(m+1)}}{\nu(1+\delta_{nm})}Re\left\{E_{mn}(r)\right\}(1-\delta_{n0}-\delta_{n1})\\&\times\sum_{j=1}^{[n/2]}(2n-4j+1)\sum_{s=|n-m-2j|}^{n+m-2j}S_{nmjs}\delta_{ks},\end{aligned} \tag{B28}$$

$$j_{\min}=\begin{cases}|n-m|\ \text{for}\ n\neq m,\\1\ \text{for}\ n=m,\end{cases} \tag{B29}$$

$$S_{nmjs}=\begin{cases}0\ \text{for}\ s=0,\\\dfrac{C_{(n-2j)0m0}^{s0}C_{(n-2j)0m1}^{s1}}{\sqrt{s(s+1)}}\ \text{for}\ s\neq 0.\end{cases} \tag{B30}$$

Equation (B25) suggests that $\boldsymbol{\Psi}^{(nm)}$ should be sought as

$$\boldsymbol{\Psi}^{(nm)}=\boldsymbol{e}_\varepsilon\sum_{k=1}^{n+m}\Psi_k^{(nm)}(r)P_k^1(\mu). \tag{B31}$$

Substitution of Eq. (B31) into Eq. (B25) yields

$$\begin{aligned}&\Psi_k^{(nm)IV}(r)+\frac{4}{r}\Psi_k^{(nm)///}(r)-\frac{2k(k+1)}{r^2}\Psi_k^{(nm)//}(r)\\&+\frac{k(k-1)(k+1)(k+2)}{r^4}\Psi_k^{(nm)}(r)=G_k^{(nm)}(r).\end{aligned} \tag{B32}$$

According to the method of variation of constants,[53] a solution to Eq. (B32) is written by

$$\Psi_k^{(nm)}(r)=\frac{C_{3k}^{(nm)}(r)}{r^{k-1}}+\frac{C_{4k}^{(nm)}(r)}{r^{k+1}}+r^kC_{5k}^{(nm)}(r)+r^{k+2}C_{6k}^{(nm)}(r), \tag{B33}$$

where the functions $C_{3k}^{(nm)}(r)$ – $C_{6k}^{(nm)}(r)$ obey the following equations:

$$\begin{aligned}&r^{-(k-1)}C_{3k}^{(nm)\prime}+r^{-(k+1)}C_{4k}^{(nm)\prime}+r^kC_{5k}^{(nm)\prime}+r^{k+2}C_{6k}^{(nm)\prime}=0,\\&(k-1)r^{-k}C_{3k}^{(nm)\prime}+(k+1)r^{-(k+2)}C_{4k}^{(nm)\prime}\\&-kr^{k-1}C_{5k}^{(nm)\prime}-(k+2)r^{k+1}C_{6k}^{(nm)\prime}=0,\\&k(k-1)r^{-(k+1)}C_{3k}^{(nm)\prime}+(k+1)(k+2)r^{-(k+3)}C_{4k}^{(nm)\prime}\\&+k(k-1)r^{k-2}C_{5k}^{(nm)\prime}+(k+1)(k+2)r^kC_{6k}^{(nm)\prime}=0,\\&k(k^2-1)r^{-(k+2)}C_{3k}^{(nm)\prime}+(k+1)(k+2)(k+3)r^{-(k+4)}\\&\times C_{4k}^{(nm)\prime}-k(k-1)(k-2)r^{k-3}C_{5k}^{(nm)\prime}\\&-k(k+1)(k+2)r^{k-1}C_{6k}^{(nm)\prime}=-G_k^{(nm)}(r).\end{aligned} \tag{B34}$$

It follows from system (B34) that

$$C_{3k}^{(nm)}(r)=C_{3k0}^{(nm)}+\frac{1}{2(2k-1)(2k+1)}\int_{R_0}^{r}s^{k+2}G_k^{(nm)}(s)ds, \tag{B35}$$

$$C_{4k}^{(nm)}(r)=C_{4k0}^{(nm)}-\frac{1}{2(2k+1)(2k+3)}\int_{R_0}^{r}s^{k+4}G_k^{(nm)}(s)ds, \tag{B36}$$

$$C_{5k}^{(nm)}(r)=C_{5k0}^{(nm)}-\frac{1}{2(2k-1)(2k+1)}\int_{R_0}^{r}s^{3-k}G_k^{(nm)}(s)ds, \tag{B37}$$

$$C_{6k}^{(nm)}(r)=C_{6k0}^{(nm)}+\frac{1}{2(2k+1)(2k+3)}\int_{R_0}^{r}s^{1-k}G_k^{(nm)}(s)ds, \tag{B38}$$

where $C_{3k0}^{(nm)}$ – $C_{6k0}^{(nm)}$ are the constants to be determined by boundary conditions.

Substituting Eqs. (B9) and (B31) into Eq. (36), one obtains the components of the Eulerian streaming velocity $\boldsymbol{v}_E^{(nm)} = \langle \boldsymbol{v}_2 \rangle^{(nm)}$,

$$v_{Er}^{(nm)}(r,\theta) = \langle v_{2r} \rangle^{(nm)} = \sum_{k=1}^{n+m} \left[\Phi_k^{(nm)/}(r) - \frac{k(k+1)}{r} \Psi_k^{(nm)}(r) \right] P_k(\mu), \tag{B39}$$

$$v_{E\theta}^{(nm)}(r,\theta) = \langle v_{2\theta} \rangle^{(nm)} = \sum_{k=1}^{n+m} \left[\frac{\Phi_k^{(nm)}(r) - \Psi_k^{(nm)}(r)}{r} - \Psi_k^{(nm)/}(r) \right] P_k^1(\mu), \tag{B40}$$

where, as follows from Eqs. (B11)–(B13) and (B33)–(B38), $\Phi_k^{(nm)/}(r)$ and $\Psi_k^{(nm)/}(r)$ are calculated by

$$\Phi_k^{(nm)/}(r) = -\frac{(k+1)C_{1k}^{(nm)}(r)}{r^{k+2}} + kr^{k-1}C_{2k}^{(nm)}(r), \tag{B41}$$

$$\Psi_k^{(nm)/}(r) = -\frac{(k-1)C_{3k}^{(nm)}(r)}{r^k} - \frac{(k+1)C_{4k}^{(nm)}(r)}{r^{k+2}} + kr^{k-1}C_{5k}^{(nm)}(r) + (k+2)r^{k+1}C_{6k}^{(nm)}(r). \tag{B42}$$

APPENDIX C: STOKES DRIFT VELOCITY PRODUCED BY MODES N AND M

The Stokes drift velocity is defined by[20]

$$\boldsymbol{v}_S = \left\langle \left(\int \boldsymbol{v}_1 dt \cdot \nabla \right) \boldsymbol{v}_1 \right\rangle = \frac{1}{2\omega} Re\{ i\boldsymbol{v}_1 \cdot \nabla \boldsymbol{v}_1^* \}. \tag{C1}$$

Substitution of Eq. (31) into Eq. (C1) yields

$$\boldsymbol{v}_S^{(nm)} = \frac{1}{2\omega(1+\delta_{nm})} Re\{ i(\boldsymbol{v}_{1n} \cdot \nabla \boldsymbol{v}_{1m}^* + \boldsymbol{v}_{1m} \cdot \nabla \boldsymbol{v}_{1n}^*) \}. \tag{C2}$$

Equation (C2) is valid for both $n \neq m$ and $n = m$.

Equation (C2) is transformed to

$$\boldsymbol{v}_S^{(nm)} = \frac{1}{2\omega(1+\delta_{nm})} Re\left\{ i\boldsymbol{e}_r \left(v_{1nr} \frac{\partial v_{1mr}^*}{\partial r} + \frac{v_{1n\theta}}{r} \frac{\partial v_{1mr}^*}{\partial \theta} + v_{1mr} \frac{\partial v_{1nr}^*}{\partial r} + \frac{v_{1m\theta}}{r} \frac{\partial v_{1nr}^*}{\partial \theta} \right) + i\boldsymbol{e}_\theta \left(v_{1nr} \frac{\partial v_{1m\theta}^*}{\partial r} + \frac{v_{1n\theta}}{r} \frac{\partial v_{1m\theta}^*}{\partial \theta} + \frac{v_{1n\theta} v_{1mr}^*}{r} + v_{1mr} \frac{\partial v_{1n\theta}^*}{\partial r} + \frac{v_{1m\theta}}{r} \frac{\partial v_{1n\theta}^*}{\partial \theta} + \frac{v_{1m\theta} v_{1nr}^*}{r} \right) \right\}. \tag{C3}$$

Substitution of Eqs. (51)–(53) into Eq. (C3) yields

$$v_{Sr}^{(nm)} = \frac{1}{2\omega(1+\delta_{nm})} Re\left\{ i\left[V_n(r) V_m'^*(r) + V_m(r) V_n'^*(r) \right] P_n(\mu) \times P_m(\mu) + i \frac{U_n(r) V_m^*(r) + U_m(r) V_n^*(r)}{r} P_n^1(\mu) P_m^1(\mu), \right\} \tag{C4}$$

$$v_{S\theta}^{(nm)} = \frac{1}{2\omega(1+\delta_{nm})} Re\left\{ i\left[V_n(r) U_m'^*(r) + \frac{U_m(r) V_n^*(r)}{r} \right] P_n(\mu) \times P_m^1(\mu) + i\left[V_m(r) U_n'^*(r) + \frac{U_n(r) V_m^*(r)}{r} \right] P_m(\mu) P_n^1(\mu) - i\frac{U_m(r) U_n^*(r)}{r} \sqrt{1-\mu^2} P_n^{1/}(\mu) P_m^1(\mu) - i\frac{U_n(r) U_m^*(r)}{r} \times \sqrt{1-\mu^2} P_m^{1/}(\mu) P_n^1(\mu) \right\}, \tag{C5}$$

where $V_n(r)$ and $U_n(r)$ are calculated by Eqs. (B23) and (B24).

With the help of Eqs. (E6), (E8), and (E10)–(E13), Eqs. (C4) and (C5) are transformed to

$$v_{Sr}^{(nm)}(r,\theta) = \sum_{k=1}^{n+m} V_{Sk}^{(nm)}(r) P_k(\mu), \tag{C6}$$

$$v_{S\theta}^{(nm)}(r,\theta) = \sum_{k=1}^{n+m} U_{Sk}^{(nm)}(r) P_k^1(\mu), \tag{C7}$$

where

$$V_{Sk}^{(nm)}(r) = \frac{1}{2\omega(1+\delta_{nm})} Re\left\{ i\left[V_n(r) V_m'^*(r) + V_m(r) V_n'^*(r) \right] \sum_{j=j_{\min}}^{n+m} \times \left[C_{n0m0}^{j0} \right]^2 \delta_{kj} + i\frac{m(m+1)}{2m+1} \frac{U_n(r) V_m^*(r) + U_m(r) V_n^*(r)}{r} \times (1-\delta_{n0}) \sum_{j=1}^{[(n+1)/2]} (2n-4j+3) \times \left[\sum_{s=|m-n+2j-2|}^{m+n-2j} \left[C_{(m-1)0(n-2j+1)0}^{s0} \right]^2 \delta_{ks} - \sum_{s=|m-n+2j|}^{m+n-2j+2} \left[C_{(m+1)0(n-2j+1)0}^{s0} \right]^2 \delta_{ks} \right] \right\}, \tag{C8}$$

$$U_{Sk}^{(nm)}(r) = W_{knm}(r) + W_{kmn}(r), \tag{C9}$$

$$W_{knm}(r) = \frac{\sqrt{m(m+1)}}{2\omega(1+\delta_{nm})} Re\left\{ i\left[V_n(r) U_m'^*(r) + \frac{U_m(r)}{r} \times \left[V_n^*(r) - n^2 U_n^*(r) \right] \right] \sum_{j=j_{\min}}^{n+m} \frac{C_{n0m0}^{j0} C_{n0m1}^{j1}}{\sqrt{j(j+1)}} \delta_{kj} + i\frac{U_m(r) U_n^*(r)}{r} (1-\delta_{n0}-\delta_{n1}) \times \sum_{j=1}^{[n/2]} (2n-4j+1) \sum_{s=|n-m-2j|}^{n+m-2j} S_{nmjs} \delta_{ks} \right\}, \tag{C10}$$

$$V_n'(r) = a_n k_a^2 z_n''(k_a r) + b_n \frac{n(n+1)}{r^2} \left[z_n(k_\nu r) - k_\nu r z_n'(k_\nu r) \right], \tag{C11}$$

$$U_n'(r) = \frac{a_n}{r^2} \left[k_a r z_n'(k_a r) - z_n(k_a r) \right] + \frac{b_n}{r^2} \left[z_n(k_\nu r) - k_\nu r z_n'(k_\nu r) - (k_\nu r)^2 z_n''(k_\nu r) \right]. \tag{C12}$$

APPENDIX D: CALCULATION OF THE UNKNOWN COEFFICIENTS APPEARING IN THE EULERIAN VELOCITY FIELD

Here we describe how the unknown coefficients $C_{1k0}^{(nm)} - C_{6k0}^{(nm)}$ appearing in the formulation of the Eulerian velocity field are calculated.

From the condition that $\boldsymbol{v}_E^{(nm)} \to 0$ for $r \to \infty$ in the external fluid, using Eqs. (B13), (B38), and (B39), one obtains the constants $C_{2k0}^{(nm)}$, $C_{5k0}^{(nm)}$, and $C_{6k0}^{(nm)}$ for the external fluid,

$$C_{2k0}^{(nm)(ex)} = -\frac{1}{2k+1}\int_{R_0}^{\infty} s^{1-k} F_k^{(nm)(ex)}(s)ds, \tag{D1}$$

$$C_{5k0}^{(nm)(ex)} = \frac{1}{2(2k-1)(2k+1)}\int_{R_0}^{\infty} s^{3-k} G_k^{(nm)(ex)}(s)ds, \tag{D2}$$

$$C_{6k0}^{(nm)(ex)} = -\frac{1}{2(2k+1)(2k+3)}\int_{R_0}^{\infty} s^{1-k} G_k^{(nm)(ex)}(s)ds. \tag{D3}$$

The superscript (ex) means that the quantity should be calculated using the parameters of the external fluid.

From the condition that $\boldsymbol{v}_E^{(nm)}$ should be finite for $r \to 0$ in the internal fluid, using Eqs. (B12), (B35), and (B36), one obtains the constants $C_{1k0}^{(nm)}$, $C_{3k0}^{(nm)}$, and $C_{4k0}^{(nm)}$ for the internal fluid,

$$C_{1k0}^{(nm)(in)} = \frac{1}{2k+1}\int_{R_0}^{0} s^{k+2} F_k^{(nm)(in)}(s)ds, \tag{D4}$$

$$C_{3k0}^{(nm)(in)} = -\frac{1}{2(2k-1)(2k+1)}\int_{R_0}^{0} s^{k+2} G_k^{(nm)(in)}(s)ds, \tag{D5}$$

$$C_{4k0}^{(nm)(in)} = \frac{1}{2(2k+1)(2k+3)}\int_{R_0}^{0} s^{k+4} G_k^{(nm)(in)}(s)ds. \tag{D6}$$

The superscript (in) means that the quantity should be calculated using the parameters of the internal fluid.

In view of the identities

$$\nabla \times \left[\boldsymbol{e}_\varepsilon P_k^1(\mu) r^{-(k+1)}\right] = -k\nabla\left[P_k(\mu) r^{-(k+1)}\right], \tag{D7}$$

$$\nabla \times \left[\boldsymbol{e}_\varepsilon P_k^1(\mu) r^{k}\right] = -(k+1)\nabla\left[P_k(\mu) r^{k}\right], \tag{D8}$$

the terms $C_{1k0}^{(nm)} r^{-(k+1)}$ and $C_{2k0}^{(nm)} r^k$ in Eq. (B11) for $\Phi_k^{(nm)}$ give the same contribution to the velocity field as the terms $C_{4k0}^{(nm)} r^{-(k+1)}$ and $C_{5k0}^{(nm)} r^k$ in Eq. (B33) for $\Psi_k^{(nm)}$. In view of this fact, we can set one of the constants $C_{1k0}^{(nm)}$ and $C_{4k0}^{(nm)}$ and one of the constants $C_{2k0}^{(nm)}$ and $C_{5k0}^{(nm)}$ to zero. Since some of these constants are already determined by Eqs. (D1)–(D6), we set

$$C_{1k0}^{(nm)(ex)} = C_{2k0}^{(nm)(in)} = 0. \tag{D9}$$

In order to calculate the other constants, boundary conditions for acoustic streaming at the particle surface are applied, which are given by

$$v_{Lr}^{(nm)(ex)} = 0 \text{ at } r = R_0, \tag{D10}$$

$$v_{Lr}^{(nm)(in)} = 0 \text{ at } r = R_0, \tag{D11}$$

$$v_{L\theta}^{(nm)(ex)} = v_{L\theta}^{(nm)(in)} \text{ at } r = R_0, \tag{D12}$$

$$\sigma_{Lr\theta}^{(nm)(ex)} = \sigma_{Lr\theta}^{(nm)(in)} \text{ at } r = R_0, \tag{D13}$$

where $v_{Lr}^{(nm)(ex,in)}$ and $v_{L\theta}^{(nm)(ex,in)}$ are the components of the Lagrangian streaming velocity in the external and internal fluids, respectively, and $\sigma_{Lr\theta}^{(nm)(ex,in)}$ is the tangential stress produced by the Lagrangian streaming in the external and internal fluids, respectively, which is given by

$$\sigma_{Lr\theta}^{(nm)(ex,in)} = \eta^{(ex,in)}\left(\frac{1}{r}\frac{\partial v_{Lr}^{(nm)(ex,in)}}{\partial\theta} + \frac{\partial v_{L\theta}^{(nm)(ex,in)}}{\partial r} - \frac{v_{L\theta}^{(nm)(ex,in)}}{r}\right). \tag{D14}$$

From Eqs. (D10)–(D13), one obtains

$$k(k+1)R_0^2 C_{3k0}^{(nm)(ex)} + k(k+1)C_{4k0}^{(nm)(ex)} = Q_{1k}^{(nm)}, \tag{D15}$$

$$k(k+1)R_0^{2k+1} C_{5k0}^{(nm)(in)} + k(k+1)R_0^{2k+3} C_{6k0}^{(nm)(in)} = Q_{2k}^{(nm)}, \tag{D16}$$

$$\begin{aligned}&(k-2)R_0^2 C_{3k0}^{(nm)(ex)} + kC_{4k0}^{(nm)(ex)} + (k+1)R_0^{2k+1} C_{5k0}^{(nm)(in)}\\ &+ (k+3)R_0^{2k+3} C_{6k0}^{(nm)(in)} = Q_{3k}^{(nm)},\end{aligned} \tag{D17}$$

$$\begin{aligned}&2\eta^{(ex)}(k^2-1)R_0^2 C_{3k0}^{(nm)(ex)} + 2\eta^{(ex)}k(k+2)C_{4k0}^{(nm)(ex)}\\ &- 2\eta^{(in)}(k^2-1)R_0^{2k+1} C_{5k0}^{(nm)(in)}\\ &- 2\eta^{(in)}k(k+2)R_0^{2k+3} C_{6k0}^{(nm)(in)} = Q_{4k}^{(nm)},\end{aligned} \tag{D18}$$

where

$$\begin{aligned}Q_{1k}^{(nm)} &= R_0^{k+2} V_{Sk}^{(nm)(ex)}(R_0) + kR_0^{2k+1}\left[C_{2k0}^{(nm)(ex)}\right.\\ &\left. - (k+1)C_{5k0}^{(nm)(ex)} - (k+1)R_0^2 C_{6k0}^{(nm)(ex)}\right],\end{aligned} \tag{D19}$$

$$\begin{aligned}Q_{2k}^{(nm)} &= R_0^{k+2} V_{Sk}^{(nm)(in)}(R_0) - (k+1)\left[C_{1k0}^{(nm)(in)}\right.\\ &\left. + kR_0^2 C_{3k0}^{(nm)(in)} + kC_{4k0}^{(nm)(in)}\right],\end{aligned} \tag{D20}$$

$$\begin{aligned}Q_{3k}^{(nm)} &= R_0^{k+2}\left[U_{Sk}^{(nm)(in)}(R_0) - U_{Sk}^{(nm)(ex)}(R_0)\right] + C_{1k0}^{(nm)(in)} + (k-2)\\ &\times R_0^2 C_{3k0}^{(nm)(in)} + kC_{4k0}^{(nm)(in)} + R_0^{2k+1}\left[(k+1)C_{5k0}^{(nm)(ex)}\right.\\ &\left. + (k+3)R_0^2 C_{6k0}^{(nm)(ex)} - C_{2k0}^{(nm)(ex)}\right],\end{aligned} \tag{D21}$$

$$\begin{aligned}Q_{4k}^{(nm)} &= \eta^{(ex)} R_0^{k+2}\left[R_0 U_{Sk}^{(nm)(ex)/}(R_0) + V_{Sk}^{(nm)(ex)}(R_0) - U_{Sk}^{(nm)(ex)}(R_0)\right]\\ &- \eta^{(in)} R_0^{k+2}\left[R_0 U_{Sk}^{(nm)(in)/}(R_0) + V_{Sk}^{(nm)(in)}(R_0) - U_{Sk}^{(nm)(in)}(R_0)\right]\\ &+ 2\eta^{(in)}\left[(k+2)C_{1k0}^{(nm)(in)} + (k^2-1)R_0^2 C_{3k0}^{(nm)(in)}\right.\\ &\left. + k(k+2)C_{4k0}^{(nm)(in)}\right] + 2\eta^{(ex)} R_0^{2k+1}\left[(k-1)C_{2k0}^{(nm)(ex)}\right.\\ &\left. - (k^2-1)C_{5k0}^{(nm)(ex)} - k(k+2)R_0^2 C_{6k0}^{(nm)(ex)}\right],\end{aligned} \tag{D22}$$

and $U_{Sk}^{(nm)/}(r)$ is calculated by

$$U_{Sk}^{(nm)/}(r) = W_{knm}^{/}(r) + W_{kmn}^{/}(r), \tag{D23}$$

where

$$\begin{aligned} W_{knm}^{/}(r) = {} & \frac{\sqrt{m(m+1)}}{2\omega(1+\delta_{nm})} Re\Bigg\{ i\Bigg\{ \left[\frac{U_m^{/}(r)}{r} - \frac{U_m(r)}{r^2} \right] \\ & \times \left[V_n^*(r) - n^2 U_n^*(r) \right] + \frac{U_m(r)}{r} \left[V_n^{/*}(r) - n^2 U_n^{/*}(r) \right] \\ & + V_n(r) U_m^{//*}(r) + V_n^{/}(r) U_m^{/*}(r) \Big\} \sum_{j=j_{\min}}^{n+m} \frac{C_{n0m0}^{j0} C_{n0m1}^{j1}}{\sqrt{j(j+1)}} \delta_{kj} \\ & + i\Bigg\{ \frac{U_m^{/}(r) U_n^*(r)}{r} + U_m(r) \left[\frac{U_n^{/*}(r)}{r} - \frac{U_n^*(r)}{r^2} \right] \Bigg\} \\ & \times (1 - \delta_{n0} - \delta_{n1}) \sum_{j=1}^{[n/2]} (2n - 4j + 1) \sum_{s=|n-m-2j|}^{n+m-2j} S_{nmjs} \delta_{ks} \Bigg\}, \end{aligned} \tag{D24}$$

$$\begin{aligned} U_n^{//}(r) = {} & \frac{a_n}{r^3} \left[(k_a r)^2 z_n^{//}(k_a r) - 2k_a r z_n^{/}(k_a r) + 2 z_n(k_a r) \right] \\ & - \frac{b_n}{r^3} \left[(k_v r)^3 z_n^{///}(k_v r) + (k_v r)^2 z_n^{//}(k_v r) \right. \\ & \left. - 2k_v r z_n^{/}(k_v r) + 2 z_n(k_v r) \right]. \end{aligned} \tag{D25}$$

Equations (D23)–(D25) are applied to both the external and the internal fluids by using quantities that correspond to, respectively, the external or the internal fluid.

From Eqs. (D15)–(D18), it follows that

$$\begin{aligned} C_{3k0}^{(nm)(ex)} = {} & \frac{1}{2k(k+1)(2k+1)(\eta^{(ex)} + \eta^{(in)}) R_0^2} \Bigg\{ \Big[2(k+2)\eta^{(ex)} \\ & + (2k+1)\eta^{(in)} \Big] k Q_{1k}^{(nm)} + \eta^{(in)}(k+1) \Big[3Q_{2k}^{(nm)} \\ & - k(2k+1) Q_{3k}^{(nm)} \Big] - k(k+1) Q_{4k}^{(nm)} \Bigg\}, \end{aligned} \tag{D26}$$

$$\begin{aligned} C_{4k0}^{(nm)(ex)} = {} & -\frac{1}{2k(k+1)(2k+1)(\eta^{(ex)} + \eta^{(in)})} \Bigg\{ \Big[2(k^2-1)\eta^{(ex)} \\ & + (k-2)(2k+1)\eta^{(in)} \Big] Q_{1k}^{(nm)} + \eta^{(in)}(k+1) \\ & \times \Big[3Q_{2k}^{(nm)} - k(2k+1) Q_{3k}^{(nm)} \Big] - k(k+1) Q_{4k}^{(nm)} \Bigg\}, \end{aligned} \tag{D27}$$

$$\begin{aligned} C_{5k0}^{(nm)(in)} = {} & -\frac{1}{2k(k+1)(2k+1)(\eta^{(ex)} + \eta^{(in)}) R_0^{2k+1}} \Bigg\{ 3k\eta^{(ex)} Q_{1k}^{(nm)} \\ & - \Big[(2k+1)(k+3)\eta^{(ex)} + 2k(k+2)\eta^{(in)} \Big] Q_{2k}^{(nm)} \\ & + k(k+1) \Big[(2k+1)\eta^{(ex)} Q_{3k}^{(nm)} - Q_{4k}^{(nm)} \Big] \Bigg\}, \end{aligned} \tag{D28}$$

$$\begin{aligned} C_{6k0}^{(nm)(in)} = {} & \frac{1}{2k(k+1)(2k+1)(\eta^{(ex)} + \eta^{(in)}) R_0^{2k+3}} \Bigg\{ 3k\eta^{(ex)} Q_{1k}^{(nm)} \\ & - \Big[(2k+1)\eta^{(ex)} + 2(k-1)\eta^{(in)} \Big] (k+1) Q_{2k}^{(nm)} \\ & + k(k+1) \Big[(2k+1)\eta^{(ex)} Q_{3k}^{(nm)} - Q_{4k}^{(nm)} \Big] \Bigg\}. \end{aligned} \tag{D29}$$

The calculation of the constants is completed and hence the calculation of the acoustic streaming is completed as well.

APPENDIX E: MATHEMATICAL IDENTITIES USED IN DERIVATION

We use the following formulas for $P_n(\mu)$ and $P_n^1(\mu)$:[52]

$$P_n^1(\mu) = -\sqrt{1-\mu^2} P_n^{/}(\mu), \tag{E1}$$

$$(1-\mu^2) P_n^{/}(\mu) = \frac{n(n+1)}{2n+1} [P_{n-1}(\mu) - P_{n+1}(\mu)], \tag{E2}$$

$$P_n^{/}(\mu) = \sum_{j=1}^{[(n+1)/2]} (2n - 4j + 3) P_{n-2j+1}(\mu), \tag{E3}$$

$$\mu P_n^{/}(\mu) = n P_n(\mu) + P_{n-1}^{/}(\mu), \tag{E4}$$

$$\sqrt{1-\mu^2} P_n^{1/}(\mu) = n(n+1) P_n(\mu) - \mu P_n^{/}(\mu), \tag{E5}$$

where [ ] in the upper bound of the sum means the integer part of an expression inside the brackets.

With the help of these formulas, the following identities are derived:

$$\begin{aligned} P_n^1(\mu) P_m^1(\mu) = {} & \frac{m(m+1)}{2m+1} [P_{m-1}(\mu) - P_{m+1}(\mu)] \\ & \times \sum_{j=1}^{[(n+1)/2]} (2n - 4j + 3) P_{n-2j+1}(\mu), \end{aligned} \tag{E6}$$

$$\begin{aligned} & \frac{\mu}{\sqrt{1-\mu^2}} P_n^1(\mu) + \sqrt{1-\mu^2} P_n^{1/}(\mu) \\ & = n(n-1) P_n(\mu) - 2 \sum_{j=1}^{[n/2]} (2n - 4j + 1) P_{n-2j}(\mu), \end{aligned} \tag{E7}$$

$$\sqrt{1-\mu^2} P_n^{1/}(\mu) = n^2 P_n(\mu) - \sum_{j=1}^{[n/2]} (2n - 4j + 1) P_{n-2j}(\mu). \tag{E8}$$

Equation (9) of § 5.6 of Ref. 54 gives the following identity:

$$\begin{aligned} P_{n_1}^{m_1}(\mu) P_{n_2}^{m_2}(\mu) = {} & \sqrt{\frac{(n_1+m_1)!(n_2+m_2)!}{(n_1-m_1)!(n_2-m_2)!}} \sum_{j=|n_1-n_2|}^{n_1+n_2} \sqrt{\frac{(j-m_1-m_2)!}{(j+m_1+m_2)!}} \\ & \times C_{n_1 0 n_2 0}^{j0} C_{n_1 m_1 n_2 m_2}^{j(m_1+m_2)} P_j^{m_1+m_2}(\mu), \end{aligned} \tag{E9}$$

where $C_{n_1 m_1 n_2 m_2}^{n_3 m_3} = \langle n_1 m_1 n_2 m_2 | n_3 m_3 \rangle$ are the Clebsch–Gordan coefficients,[52,55] which are zero unless the following conditions are satisfied: $m_3 = m_1 + m_2$, $n_1 + n_2 - n_3 \geq 0$, $n_1 - n_2 + n_3 \geq 0$, $-n_1 + n_2 + n_3 \geq 0$, $|m_1| \leq n_1$, $|m_2| \leq n_2$, and $|m_3| \leq n_3$.

From Eq. (E9), one obtains

$$P_n(\mu) P_m(\mu) = \sum_{j=|n-m|}^{n+m} \left[C_{n0m0}^{j0} \right]^2 P_j(\mu), \tag{E10}$$

$$P_{m-1}(\mu) P_{n-2j+1}(\mu) = \sum_{s=|m-n+2j-2|}^{m+n-2j} \left[C_{(m-1)0(n-2j+1)0}^{s0} \right]^2 P_s(\mu), \tag{E11}$$

$$P_{m+1}(\mu)P_{n-2j+1}(\mu) = \sum_{s=|m-n+2j|}^{m+n-2j+2} \left[C^{s0}_{(m+1)0(n-2j+1)0}\right]^2 P_s(\mu), \quad \text{(E12)}$$

$$P_n(\mu)P^1_m(\mu) = \sqrt{m(m+1)} \sum_{j=|n-m|}^{n+m} \frac{C^{j0}_{n0m0}C^{j1}_{n0m1}}{\sqrt{j(j+1)}} P^1_j(\mu). \quad \text{(E13)}$$

REFERENCES

[1]W. L. Nyborg, "Biological effects of ultrasound: Development of safety guidelines. Part II: General review," Ultrasound Med. Biol. **27**, 301–333 (2001).
[2]P. Marmottant and S. Hilgenfeldt, "Controlled vesicle deformation and lysis by single oscillating bubbles," Nature **423**, 153–156 (2003).
[3]R. H. Liu, J. Hang, M. Z. Pindera, M. Athavale, and P. Grodzinski, "Bubble-induced acoustic micromixing," Lab Chip **2**, 151–157 (2002).
[4]J. Friend and L. Y. Yeo, "Microscale acoustofluidics: Microfluidics driven via acoustics and ultrasonics," Rev. Mod. Phys. **83**, 647–704 (2011).
[5]M. Wiklund, R. Green, and M. Ohlin, "Acoustofluidics 14: Applications of acoustic streaming in microfluidic devices," Lab Chip **12**, 2438–2451 (2012).
[6]R. Manasseh, "Acoustic bubbles, acoustic streaming, and cavitation microstreaming," in *Handbook of Ultrasonics and Sonochemistry*, edited by M. Ashokkumar (Springer, Singapore, 2016), pp. 33–68.
[7]P. Zhang, H. Bachman, A. Ozcelik, and T. J. Huang, "Acoustic microfluidics," Annu. Rev. Anal. Chem. **13**, 17–43 (2020).
[8]J. Rufo, F. Cai, J. Friend, M. Wiklund, and T. J. Huang, "Acoustofluidics for biomedical applications," Nat. Rev. Methods Primers **2**, 30 (2022).
[9]J. Friend, "Acoustofluidics," Front. Acoust. **1**, 1261027 (2023).
[10]W. Wei, Y. Wang, Z. Wang, and X. Duan, "Microscale acoustic streaming for biomedical and bioanalytical applications," TrAC Trends Anal. Chem. **160**, 116958 (2023).
[11]W. L. Nyborg, "Acoustic streaming," in *Physical Acoustics*, edited by W. P. Mason (Academic, New York, 1965), Vol. IIB, pp. 266–331.
[12]J. Lighthill, "Acoustic streaming," J. Sound Vib. **61**, 391–418 (1978).
[13]C. A. Lane, "Acoustical streaming in the vicinity of a sphere," J. Acoust. Soc. Am. **27**, 1082–1086 (1955).
[14]C.-Y. Wang, "The flow field induced by an oscillating sphere," J. Sound Vib. **2**, 257–269 (1965).
[15]N. Riley, "On a sphere oscillating in a viscous liquid," Q. J. Mech. Appl. Math. **19**, 461–472 (1966).
[16]A. Gopinath, "Steady streaming due to small-amplitude torsional oscillations of a sphere in a viscous fluid," Q. J. Mech. Appl. Math. **46**, 501–520 (1993).
[17]A. Gopinath, "Steady streaming due to small-amplitude superposed oscillations of a sphere in a viscous fluid," Q. J. Mech. Appl. Math. **47**, 461–480 (1994).
[18]B. J. Davidson and N. Riley, "Cavitation microstreaming," J. Sound Vib. **15**, 217–233 (1971).
[19]J. Wu and G. Du, "Streaming generated by a bubble in an ultrasound field," J. Acoust. Soc. Am. **101**, 1899–1907 (1997).
[20]M. S. Longuet-Higgins, "Viscous streaming from an oscillating spherical bubble," Proc. R. Soc. London, Ser. A **454**, 725–742 (1998).
[21]A. O. Maksimov, "Viscous streaming from surface waves on the wall of acoustically-driven gas bubbles," Eur. J. Mech. B/Fluids **26**, 28–42 (2007).
[22]T. A. Spelman and E. Lauga, "Arbitrary axisymmetric steady streaming: Flow, force and propulsion," J. Eng. Math. **105**, 31–65 (2017).
[23]A. A. Doinikov, S. Cleve, G. Regnault, C. Mauger, and C. Inserra, "Acoustic microstreaming produced by nonspherical oscillations of a gas bubble. I. Case of modes 0 and m," Phys. Rev. E **100**, 033104 (2019).
[24]A. A. Doinikov, S. Cleve, G. Regnault, C. Mauger, and C. Inserra, "Acoustic microstreaming produced by nonspherical oscillations of a gas bubble. II. Case of modes 1 and m," Phys. Rev. E **100**, 033105 (2019).
[25]C. Inserra, G. Regnault, S. Cleve, C. Mauger, and A. A. Doinikov, "Acoustic microstreaming produced by nonspherical oscillations of a gas bubble. III. Case of self-interacting modes n-n," Phys. Rev. E **101**, 013111 (2020).
[26]C. Inserra, G. Regnault, S. Cleve, C. Mauger, and A. A. Doinikov, "Acoustic microstreaming produced by nonspherical oscillations of a gas bubble. IV. Case of modes n and m," Phys. Rev. E **102**, 043103 (2020).
[27]V. Pereno, M. Aron, O. Vince, C. Mannaris, A. Seth, M. de Saint Victor, G. Lajoinie, M. Versluis, C. Coussios, D. Carugo, and E. Stride, "Layered acoustofluidic resonators for the simultaneous optical and acoustic characterization of cavitation dynamics, microstreaming and biological effects," Biomicrofluidics **12**, 034109 (2018).
[28]P. Tho, R. Manasseh, and A. Ooi, "Cavitation microstreaming patterns in single and multiple bubble systems," J. Fluid Mech. **576**, 191–233 (2007).
[29]S. Cleve, M. Guedra, C. Mauger, C. Inserra, and P. Blanc-Benon, "Microstreaming induced by acoustically-trapped, non-spherically oscillating microbubbles," J. Fluid Mech. **875**, 597–621 (2019).
[30]G. Regnault, C. Mauger, P. Blanc-Benon, A. A. Doinikov, and C. Inserra, "Signature of microstreaming patterns induced by non-spherically oscillating bubbles," J. Acoust. Soc. Am. **150**(2), 1188–1197 (2021).
[31]X. Liu and J. Wu, "Acoustic microstreaming around an isolated encapsulated microbubble," J. Acoust. Soc. Am. **125**, 1319–1330 (2009).
[32]A. A. Doinikov and A. Bouakaz, "Acoustic microstreaming around a gas bubble," J. Acoust. Soc. Am. **127**, 703–709 (2010).
[33]M. Cattaneo, G. Guerriero, G. Shakya, L. A. Krattiger, L. G. Paganella, M. L. Narciso, and O. Supponen, "Cyclic jetting enables microbubble-mediated drug delivery," Nat. Phys. **21**, 590–598 (2025).
[34]K. Sritharan, C. J. Strobl, M. F. Schneider, and A. Wixforth, "Acoustic mixing at low Reynolds numbers," Appl. Phys. Lett. **88**, 054102 (2006).
[35]A. Riaud, M. Baudoin, O. Bou Matar, J. L. Thomas, and P. Brunet, "On the influence of viscosity and caustics on acoustic streaming in sessile droplets: An experimental and a numerical study with a cost-effective method," J. Fluid Mech. **821**, 384–420 (2017).
[36]S. Collignon, J. R. Friend, and L. Y. Yeo, "Planar microfluidic drop splitting and merging," Lab Chip **15**, 1942–3288 (2015).
[37]M. K. Tan, J. R. Friend, and L. Y. Yeo, "Interfacial jetting phenomena induced by focused surface vibrations," Phys. Rev. Lett. **103**(2), 024501 (2009).
[38]A. Qi, L. Y. Yeo, and J. R. Friend, "Interfacial destabilization and atomization driven by surface acoustic waves," Phys. Fluids **20**(7), 074103 (2008).
[39]E. Trinh, A. Zwern, and T. G. Wang, "An experimental study of small-amplitude drop oscillations in immiscible liquid systems," J. Fluid Mech. **115**, 453–474 (1982).
[40]C. L. Shen, W. J. Xie, Z. L. Yan, and B. Wei, "Internal flow of acoustically levitated drops undergoing sectorial oscillations," Phys. Lett. A **374**, 4045–4048 (2010).
[41]Y. Yamamoto, Y. Abe, A. Fujiwara, K. Hasegawa, and K. Aoki, "Internal flow of acoustically levitated droplet," Microgravity Sci. Technol. **20**, 277–280 (2008).
[42]Z. Zapryanov and S. Stoyanova, "The flow field induced by an oscillating fluid drop immersed in another fluid," Int. J. Multiphase Flow **4**, 193–201 (1978).
[43]H. Zhao, S. S. Sadhal, and E. H. Trinh, "Internal circulation in a drop in an acoustic field," J. Acoust. Soc. Am. **106**, 3289–3295 (1999).
[44]A. Y. Rednikov, H. Zhao, and S. S. Sadhal, "Steady streaming around a spherical drop displaced from the velocity antinode in an acoustic levitation field," Q. J. Mech. Appl. Math. **59**, 377–397 (2006).
[45]T. Baasch, A. A. Doinikov, and J. Dual, "Acoustic streaming outside and inside a fluid particle undergoing monopole and dipole oscillations," Phys. Rev. E **101**, 013108 (2020).
[46]A. L. Yarin, "Stationary d.c. streaming due to shape oscillations of a droplet and its effect on mass transfer in liquid-liquid systems," J. Fluid Mech. **444**, 321–342 (2001).
[47]H. Schlichting, *Boundary-Layer Theory* (McGraw-Hill, New York, 1979).
[48]L. D. Landau and E. M. Lifshitz, *Fluid Mechanics* (Pergamon Press, Oxford, 1987).
[49]T. G. Leighton, D. G. H. Coles, M. Srokosz, P. R. White, and D. K. Woolf, "Asymmetric transfer of CO_2 across a broken sea surface," Sci. Rep. **8**, 8301 (2018).
[50]M. Versluis, E. Stride, G. Lajoinie, B. Dollet, and T. Segers, "Ultrasound contrast agent modelling: A review," Ultrasound Med. Biol. **46**(9), 2117–2144 (2020).
[51]S. J. Putterman and K. R. Weninger, "Sonoluminescence: How bubbles turn sound into light," Annu. Rev. Fluid Mech. **32**, 445–476 (2000).
[52]M. Abramowitz and I. A. Stegun, *Handbook of Mathematical Functions with Formulas, Graphs and Mathematical Tables* (Dover Publication, Dover, New York, 1972).
[53]W. E. Boyce and R. C. DiPrima, *Elementary Differential Equations and Boundary Value Problems* (Wiley, New York, 2001).
[54]D. A. Varshalovich, A. N. Moskalev, and V. K. Khersonskii, *Quantum Theory of Angular Momentum* (World Scientific, Teaneck, NJ, 1988).
[55]D. Zwillinger, *Standard Mathematical Tables and Formulae* (CRC, Boca Raton, 2003).